

**Synthesis and Investigation of
Electrical and Magnetic Properties of
Co-Ni Substituted Spinel Ferrites
Nanoparticles**



**By
Sobaan Naseer**

**School of Chemical and Materials Engineering
National University of Sciences and Technology**

2023

**Synthesis and Investigation of
Electrical and Magnetic Properties of
Co-Ni Substituted Spinel Ferrites
Nanoparticles**



Name: Sobaan Naseer

Registration No: 00000329738

**This thesis is submitted as a partial fulfillment of the requirements
for the degree of
MS in Nanoscience and Engineering**

Supervisor Name: Prof. Dr. Iftikhar Hussain Gul

**School of Chemical and Materials Engineering (SCME)
National University of Sciences and Technology (NUST)
H-12 Islamabad, Pakistan**

January 2023



THESIS ACCEPTANCE CERTIFICATE

Certified that final copy of MS thesis written by Mr **Sobaan Naseer** (Registration No 00000329738), of School of Chemical & Materials Engineering (SCME) has been vetted by undersigned, found complete in all respects as per NUST Statues/Regulations, is free of plagiarism, errors, and mistakes and is accepted as partial fulfillment for award of MS degree. It is further certified that necessary amendments as pointed out by GEC members of the scholar have also been incorporated in the said thesis.


Signature: _____ 

Name of Supervisor: **Dr Iftikhar Hussian Gul**

Date: 09/01/2023

Signature (HOD): _____ 

Date: 18/8/23

Signature (Dean/Principal): _____ 

Date: 18.8.2023





Form TH-1

(Must be type written)

National University of Sciences & Technology (NUST)

MASTER'S THESIS WORK

Formulation of Guidance and Examination Committee (GEC)

Name: **Sobaan Naseer**

NUST Reg No: **00000329738**

Department: **Materials Engineering**

Specialization: **Nanoscience Engineering**

Credit Hour Completed: **26**

CGPA: **3.06**

Course Work Completed

S/No	Code	Title	Core/Elective	CH	Grade
1	RM-898	Research Methodology	Additional	2	Q
2	NSE-813	Essentials of Nanoscience and Engineering	Core	3	B
3	MSE-854	Characterization Of Materials	Core	3	B+
4	NSE-845	Nanolithography And Device Fabrication	Elective	3	B+
5	MSE-856	Nano Material and Processing	Core	3	C+
6	MSE-872	Composite Materials	Elective	3	B
7	NSE-812	Environmental Nanotechnology	Elective	3	C+
8	NSE-961	Surface Coatings and Thin Films	Elective	3	B+
9	ESE-829	Functional Nanomaterials for Renewable Energy	Elective	3	B

Exam 31
10/5/22

Date: 29th May 2022

Student's Signature: [Signature]

Thesis Committee

- Name: **Dr. Iftikhar Hussain Gul (Supervisor)**
Department: **Materials Engineering**
- Name: **Dr. Nasir Ahmad (Member)**
Department: **Materials Engineering**
- Name: **Dr. Usman Liaqat (Member)**
Department: **Materials Engineering**

Signature: [Signature]

Signature: [Signature]

Signature: [Signature]

Date: 30.05.22

Signature of Head of Department: [Signature]

APPROVAL

Date: 30.5.2022

[Signature]
Dean/Principal

Distribution

- 1x copy to Exam Branch, Main Office NUST
- 1x copy to PGP Dte, Main Office NUST
- 1x copy to Exam branch, respective institute

School of Chemical and Materials Engineering (SCME) Sector H-12, Islamabad



FORM TH-4

MASTER'S THESIS WORK

We hereby recommend that the dissertation prepared under our supervision by

Regn No & Name: 00000329738 Sobaan Naseer

Title: Synthesis & Investigation of Electrical & Magnetic Properties of Co-Ni Substituted Spinel Ferrites Nanoparticle.

Presented on: 13 Apr 2023 at: 1400 hrs in SCME Seminar Hall

Be accepted in partial fulfillment of the requirements for the award of Masters of Science degree in Nanoscience & Engineering.

Guidance & Examination Committee Members

Name: Dr Nasir M Ahmad

Signature:

Name: Dr Usman Liaqat

Signature:

Supervisor's Name: Dr Iftikhar Hussain Gul

Signature:
Dated: 13/4/23

Head of Department

Date 14-4-23

Dean/Principal

Date 14.4.23

Dedications

I dedicate this thesis to my beloved Family for their unconditional support and love.

Acknowledgements

All admiration to Allah Almighty. He is the One, who bestows and gives the power to us to think, utilize our expertise in knowledge in achieving remarkable solutions for mankind in every field. Therefore, I express my greatest thanks to Almighty Allah the universal and the architect of the world. Allah Almighty says in Quran:

“Read! In the name of your lord” (Alaq; 1st revealed ayah)

This Quranic verse sums up the entire importance of education in the lives of humans.

I like to express my gratefulness to my very supportive and respected supervisor **Prof. Dr. Iftikhar Hussain Gul** for his clear and patient guidance that directed me to fulfill my project and this thesis. His cool and calm behavior motivated me to do my best. His valuable suggestions, constructive advice and feedback contributed to this thesis. Also, I am very grateful to my GEC members including **Dr. Usman Liaqat** and **Prof. Dr. Nasir Mahmood Ahmad** who helped me and motivated me to do my best. I would also like to thank my parents, family members, and friends for their help, prayers, and their valuable suggestions.

I also want to especially thank **Ms. Varda Shakeel** and **Ms. Anoom Zafar** for their support as they helped a lot during characterization and lab work.

I acknowledge the support provided by the Materials Engineering Department of SCME for providing me with a platform to perform my experiments and use my skills in research work.

I acknowledge the financial aid and technical assistance provided by our department, SCME, during my research experience made this project work memorable forever.

- **Sobaan Naseer**

Abstract

The nanocomposite of spinel ferrites and multi walled carbon nanotubes (MWCNTs) is synthesized and structural, electrical, and magnetic properties were investigated. Zinc and Nickel substituted Cobalt ferrites were prepared using the simple and economical method of nanoparticles synthesis called Co-precipitation. A nanocomposite is achieved by coating MWCNTs with ferrites using toluene as a dispersive medium. Different loadings of the MWCNTs have been applied to see the effect of MWCNTs on the magnetic and dielectric properties. The loadings applied were 0%, 0.25%, 0.50%, 0.75% and 1%. The prepared nanocomposites were structurally characterized using X-ray diffraction and Fourier transform infrared spectroscopy. The obtained XRD patterns verified the formation of pure Face Centered Cubic single phase of $Zn_{0.2}Ni_{0.3}Co_{0.5}Fe_2O_4$ /MWCNTs nanocomposite. The average crystallite size for the zinc and nickel substituted cobalt ferrites measured by Debye-Scherrer equation was $15 \text{ nm} \pm 3 \text{ nm}$. The average crystallite size for each sample was in complete agreement with the results obtained from high resolution scanning electron microscope within experimental error. Scanning electron microscope results showed aggregation of ferrite nanoparticles on MWCNTs. The dielectric properties were analyzed and enhanced via the addition of MWCNTs. The dielectric constant of pure Zinc and Nickel substituted Cobalt ferrites was 1×10^5 whereas it was increased with the addition of MWCNTs. At wt. 1% MWCNTs, the dielectric constant was increased to 3.75×10^8 at frequency of 100 Hz. The A.C conductivity is maximum at lower frequency which represents the dominance of band conductivity over hopping conductivity. DC electrical conductivity of nanocomposites were also measured and is observed to increase with the increase in loading percentage of MWCNTs proving the conductive behavior of MWCNTs. VSM analyses the magnetization saturation of nanoparticles which turns out to be 63.7 emu/g for $Zn_{0.2}Ni_{0.3}Co_{0.5}Fe_2O_4$ nanoparticles and 35.1 emu/g for $Zn_{0.2}Ni_{0.3}Co_{0.5}Fe_2O_4$ /1% wt. MWCNTs nanocomposite.

Table of Contents

Dedications.....	i
Acknowledgements	ii
Abstract	iii
Table of Contents.....	iv
List of Figures	viii
List of Tables.....	x
List of Abbreviations.....	xi
Chapter 1 Introduction.....	1
1.1 Introduction to Nanotechnology	1
1.1.1 Importance of Nanotechnology.....	2
1.2 Classification of Nanomaterials	2
1.2.1 One-Dimensional (1-D) e.g nanowire, nanotube, etc.,	3
1.2.2 Two-Dimensional (2-D) e.g films and multilayer sheets,.....	3
1.2.3 Three-Dimensional (3-D) e.g polycrystals etc.,.....	3
1.3 Important Concepts of Nanoscience and Nanotechnology	3
1.4 Classification of Magnetic Materials	4
1.4.1 Diamagnetic Materials	4
1.4.2 Paramagnetic Materials.....	5
1.4.3 Ferromagnetic Material.....	6
1.4.4 Antiferromagnetic Materials	7
1.4.5 Ferrimagnetic Materials	7
1.5 Ferrites.....	8
1.5.1 Soft Ferrites	9
1.5.2 Hard Ferrites.....	10
1.5.3 Comparison of Soft vs Hard Magnetic.....	10
1.5.4 Structural Classification of Spinel Ferrites	10
1.5.4.1 Normal Spinel	10
1.5.4.2 Inverse Spinel.....	11
1.5.5 Why Ferrites?.....	11

1.5.6	Application of Ferrites	12
1.6	Introduction to Carbon Nanotubes	12
1.6.1	Ferrite/MWCNTs Nanocomposite	13
1.7	Objectives of My Project	14
Chapter 2 Theoretical Review		15
2.1	Nanoparticles Synthesis Methods	15
2.1.1	Top Down	15
2.1.2	Bottom Up.....	15
2.2	Some Key Approaches for Producing Oxide Nanoparticles.....	16
2.2.1	Gas Phase Condensation Methods	16
2.2.2	Microwave Plasma Processing.....	17
2.2.3	Hydrothermal Synthesis	17
2.2.4	Electric Dispersion Reaction.....	18
2.2.5	Sol-Gel (Colloidal) Processing	19
2.2.6	Sonochemical Processing.....	19
2.2.7	Spray Pyrolysis	20
2.2.8	Combustion Synthesis.....	20
2.2.9	Mechanochemical Synthesis	20
2.3	Chemical Co-Precipitation Method.....	21
2.3.1	Why Co-Precipitation Method	22
2.3.2	Steps in Co-precipitation.....	22
2.3.2.1	Co-precipitation Step	23
2.3.2.2	Ferritisation Step	23
2.3.3	Parameters Involved in Co-Precipitation:	23
2.3.3.1	Rate of Mixing of The Reactants	23
2.3.3.2	Role of Anion.....	24
2.3.3.3	Temperature Effect.....	24
2.3.3.4	Effect of pH.....	24
2.3.3.5	Heating After Co-Precipitation	25
2.4	Synthesis of Zn-Ni Substituted Co ferrite/MWCNTs Nanocomposite.....	25
2.5	Toluene as a Dispersion Medium.....	26
Chapter 3 Methodology		27

3.1	Material and Apparatus	27
3.1.1	Chemical Used	27
3.1.2	Apparatus Used	27
3.2	Co-Precipitation	28
3.2.1	Sample Processing	29
3.3	Study of Synthesized Samples	29
3.4	X-Ray Diffractions.....	29
3.4.1	Basic Principle of X-Ray Diffraction.....	30
3.4.2	Different XRD Approaches.....	30
3.4.3	Powder Diffraction Method	31
3.4.4	X-Rays Generation Explanation	31
3.5	Fourier Transform Infrared Spectroscopy (FTIR)	32
3.5.1	What Information Can FT-IR Provide?	33
3.5.2	FTIR Sample Preparation.....	33
3.6	Scanning Electron Microscope (SEM).....	33
3.6.1	How SEM Works	34
3.6.2	Precautions of SEM	35
3.6.3	SEM Sample Preparation	36
3.7	Vibrating Sample Magnetometer (VSM).....	36
3.7.1	Mechanism of VSM	36
3.7.2	Different Parts of VSM	37
3.7.2.1	Water Cooled Electromagnet	37
3.7.2.2	Sample Holder and Vibration Exciter	37
3.7.2.3	Sensor Coils and Amplifier.....	37
3.7.2.4	Lock-in Amplifier	37
3.7.2.5	Computer Interface.....	37
3.7.3	Precautions of VSM	38
3.8	Dielectric Sample Preparation.....	38
3.8.1	DC Electrical Resistivity Measurement	38
3.8.2	Dielectric Properties Measurement	39
3.9	Dielectric Loss Measurement.....	39
3.10	Tangent Loss Factor	40
3.11	AC Conductivity Measurement.....	40

3.12	AC impedance Spectroscopy	40
Chapter 4 Results and Discussion		41
4.1	XRD Analysis	41
4.2	Fourier Transform Infrared Spectroscopy	43
4.3	Scanning Electron Microscope	44
4.4	Energy Dispersive X-ray Spectrometry	47
4.5	Dielectric Properties	51
4.6	Tangent Loss Factor	53
4.7	Impedance	54
4.8	AC Conductivity	57
4.9	DC Conductivity	58
4.10	Vibrating Sample Magnetometer	59
Conclusion.....		61
References		62

List of Figures

Fig 1.1 Interdisciplinary of Nanotechnology	1
Fig 1.2 Application of Nanotechnology	2
Fig 1.3 Dimensionality of Nanomaterials	3
Fig 1.4 Scale of Nanometer (nm).....	4
Fig 1.5 Graphical Representation of Diamagnetic Material	5
Fig 1.6 Graphical Representation of Paramagnetic Material	6
Fig 1.7 Graphical Representation of Ferromagnetic Material	7
Fig 1.8 Graphical Representation of Antiferromagnetic Material	7
Fig 1.9 Graphical Representation of Ferrimagnetic Material	8
Fig 1.10 Soft vs Hard ferrites	9
Fig 1.11 Structure of Spinel Ferrites	11
Fig 1.12 Visual Representation of MWCNTs.....	12
Fig 1.13 SEM Image of MWCNTs	13
Fig 2.1 Top-Down vs Bottom-Up	15
Fig 2.2 Nanoscale Synthesis Methods	16
Fig 2.3 Flowchart of Hydrothermal Method	18
Fig 2.4 Use of Sol-Gel Technique in Synthesis of Various products	19
Fig 2.5 Visual Representation of Co-Precipitation Reaction	21
Fig 2.6 Flow Chart of Co-Precipitation Reaction	22
Fig 2.7 Toluene Chemical Structure	26
Fig 3.1 Bragg's Law Reflection as The Constructive Wave Interacts	30
Fig 3.2 Formation of Diffracted Cone	31
Fig 3.3 Visual Representation of Production of X-Rays.....	32
Fig 3.4 Working Principle of FTIR.....	33
Fig 3.5 Principle of SEM	34
Fig 3.6 Illustration of Electrons and Matter Interaction with Coated vs Uncoated Sample.....	35
Fig 3.7 Interaction of Incident Beam and Sample	35
Fig 3.8 VSM.....	36
Fig 3.9 Diagram VSM.....	38
Fig 3.10 Illustration of two-probe method instrument setup.....	39

Fig 4.1 The X-Ray diffraction Pattern of $Zn_{0.2}Ni_{0.3}Co_{0.5}Fe_2O_4$ and $Zn_{0.2}Ni_{0.3}Co_{0.5}Fe_2O_4$ MWCNTs Nanocomposites	42
Fig 4.2 The FTIR Spectra of $Zn_{0.2}Ni_{0.3}Co_{0.5}Fe_2O_4$ and $Zn_{0.2}Ni_{0.3}Co_{0.5}Fe_2O_4$ /MWCNTs Nanocomposites	43
Fig 4.3 SEM image of $Zn_{0.2}Ni_{0.3}Co_{0.5}Fe_2O_4$ Nanoparticles	45
Fig 4.4 SEM image of $Zn_{0.2}Ni_{0.3}Co_{0.5}Fe_2O_4$ / wt% 0.25 MWCNTs Nanocomposite .	45
Fig 4.5 SEM image of $Zn_{0.2}Ni_{0.3}Co_{0.5}Fe_2O_4$ / wt% 0.50 MWCNTs Nanocomposite .	45
Fig 4.6 SEM image of $Zn_{0.2}Ni_{0.3}Co_{0.5}Fe_2O_4$ / wt% 0.75 MWCNTs Nanocomposite .	46
Fig 4.7 SEM image of $Zn_{0.2}Ni_{0.3}Co_{0.5}Fe_2O_4$ / wt% 1 MWCNTs Nanocomposite	46
Fig 4.8 The EDX spectrum of $Zn_{0.2}Ni_{0.3}Co_{0.5}Fe_2O_4$	47
Fig 4.9 The EDX spectrum of $Zn_{0.2}Ni_{0.3}Co_{0.5}Fe_2O_4$ /0.25% wt MWCNTs	48
Fig 4.10 The EDX spectrum of $Zn_{0.2}Ni_{0.3}Co_{0.5}Fe_2O_4$ /0.5% wt MWCNTs	49
Fig 4.11 The EDX spectrum of $Zn_{0.2}Ni_{0.3}Co_{0.5}Fe_2O_4$ /0.75% wt MWCNTs	49
Fig 4.12 The EDX spectrum of $Zn_{0.2}Ni_{0.3}Co_{0.5}Fe_2O_4$ / 1% wt MWCNTs	50
Fig 4.13 Variation of Dielectric Constant with Frequency of $Zn_{0.2}Ni_{0.3}Co_{0.5}Fe_2O_4$ and $Zn_{0.2}Ni_{0.3}Co_{0.5}Fe_2O_4$ / MWCNTs Nanocomposites	52
Fig 4.14 Imaginary part Dielectric Constant with Frequency of $Zn_{0.2}Ni_{0.3}Co_{0.5}Fe_2O_4$ and $Zn_{0.2}Ni_{0.3}Co_{0.5}Fe_2O_4$ / MWCNTs Nanocomposites.....	53
Fig 4.15 Dielectric loss tangent as a function of Frequency of $Zn_{0.2}Ni_{0.3}Co_{0.5}Fe_2O_4$ and $Zn_{0.2}Ni_{0.3}Co_{0.5}Fe_2O_4$ / MWCNTs Nanocomposites.....	54
Fig 4.16 Variation of Z' Versus Frequency for $Zn_{0.2}Ni_{0.3}Co_{0.5}Fe_2O_4$ and $Zn_{0.2}Ni_{0.3}Co_{0.5}Fe_2O_4$ / MWCNTs Nanocomposites	55
Fig 4.17 Impedance at 100 Hz	56
Fig 4.18 Variation of Z'' Versus frequency for $Zn_{0.2}Ni_{0.3}Co_{0.5}Fe_2O_4$ and $Zn_{0.2}Ni_{0.3}Co_{0.5}Fe_2O_4$ / MWCNTs Nanocomposites	56
Fig 4.19 AC Conductivity Change as a Function of Frequency for $Zn_{0.2}Ni_{0.3}Co_{0.5}Fe_2O_4$ and $Zn_{0.2}Ni_{0.3}Co_{0.5}Fe_2O_4$ / MWCNTs Nanocomposites	57
Fig 4.20 DC Conductivity Variation with Varying wt. % MWCNTs in Ferrites	58
Fig 4.21 Magnetic Hysteresis Loop of $Zn_{0.2}Ni_{0.3}Co_{0.5}Fe_2O_4$ and $Zn_{0.2}Ni_{0.3}Co_{0.5}Fe_2O_4$ / MWCNTs Nanocomposites	59

List of Tables

Table 1 $\text{Zn}_{0.2}\text{Ni}_{0.3}\text{Co}_{0.5}\text{Fe}_2\text{O}_4$ Atomic and Weight percentage	47
Table 2 $\text{Zn}_{0.2}\text{Ni}_{0.3}\text{Co}_{0.5}\text{Fe}_2\text{O}_4/0.25\%$ wt MWCNTs Weight and Atomic percentage.	48
Table 3 $\text{Zn}_{0.2}\text{Ni}_{0.3}\text{Co}_{0.5}\text{Fe}_2\text{O}_4/0.5\%$ wt MWCNTs Weight and Atomic percentage...	49
Table 4 $\text{Zn}_{0.2}\text{Ni}_{0.3}\text{Co}_{0.5}\text{Fe}_2\text{O}_4/0.75\%$ wt MWCNTs Weight and Atomic percentage.	50
Table 5 $\text{Zn}_{0.2}\text{Ni}_{0.3}\text{Co}_{0.5}\text{Fe}_2\text{O}_4/1\%$ wt MWCNTs Weight and Atomic	50
Table 6 Table of magnetic properties of $\text{Zn}_{0.2}\text{Ni}_{0.3}\text{Co}_{0.5}\text{Fe}_2\text{O}_4$ and $\text{Zn}_{0.2}\text{Ni}_{0.3}\text{Co}_{0.5}\text{Fe}_2\text{O}_4/$ MWCNTs	60

List of Abbreviations

Acronym	Meaning
ZNCF	$Zn_{0.2}Ni_{0.3}Co_{0.5}Fe_2O_4$
EM	Electromagnetic
SWCNTs	Single walled carbon nanotubes
MWCNTs	Multi walled carbon nanotubes
MHz	Megahertz
GHz	Gigahertz
Ni	Nickel
Zn	Zinc
Co	Cobalt
SEM	Scanning electron microscopy
XRD	X-ray diffraction
VSM	Vibrating sample magnetometer
FTIR	Fourier transform infrared spectroscopy
EDX	Energy dispersive x-ray

Chapter 1

Introduction

1.1 Introduction to Nanotechnology

Today, nanotechnology is regarded as a very significant and promising technology that is working in many scientific domains for many gadgets and materials by applying various approaches at the nanoscale scale. Its name is derived from the Greek word for dwarf, nanos. The science of nanotechnology is a combination of several other sciences, including physics, biology, chemistry, electronics, materials science, etc. [1]

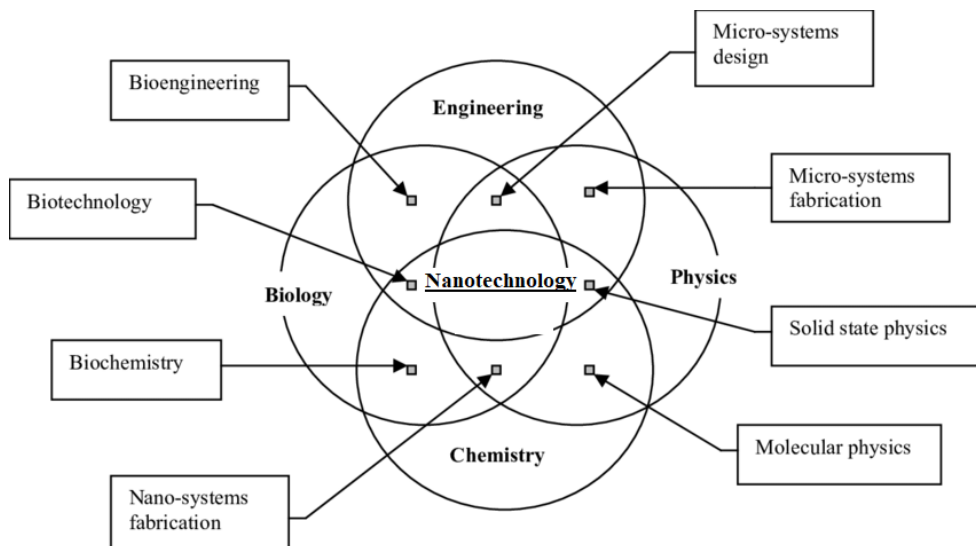


Fig 1.1 Interdisciplinary of Nanotechnology

A single particle with a diameter of between 1 and 100 nm is referred to as a nanoparticle. Due to their distinctive physicochemical characteristics, they have been widely exploited in recent years for the development of new imperative technologies. The device's miniaturization gave rise to a brand-new class of materials known as nanomaterials. "A material having particle with at least one dimension in the nanometer level about 1 to 100 nm" is the definition of a nanomaterial.

1.1.1 Importance of Nanotechnology

Nearly every element of our life is significantly influenced by nanotechnology. In our daily lives, we employ nanotechnology both deliberately and unknowingly. By making treatment techniques and tools more effective, nanotechnology is assisting researchers in their fight against fatal diseases like cancer. Water that has been contaminated is thought to be particularly dangerous to the general public's health and must be recycled before being used again. Hazardous water decontamination is a problem that exists everywhere. Nanoparticles can be utilized very successfully to remediate soil and water [2-5].

The electronic sector will likewise be significantly impacted by nanotechnology. [4-6].

Renewable energy storage applications like storing hydrogen gas are also being done by nanotechnology. Energy capture devices are also being made using nanotechnology i.e solar panels cells, and wind turbine Nano polymers [7-9].

Smart windows that can either absorb the radiation and emit it in a different form of energy, reflect the radiation or release it at a low frequency to make it less dangerous are another application of nanotechnology for UV protection [10-12].



Fig 1.2 Application of Nanotechnology

1.2 Classification of Nanomaterials

Nanomaterial is named as a material having particle size with at least one dimension

on a nanometer scale. About 1 to 100 nanometers to be accurate. These nanomaterials can be further classified according to their shape and dimensions as 0D, 1D, 2D, and 3D [13-15].

1.2.1 One-Dimensional (1-D) e.g nanowire, nanotube, etc.,

1.2.2 Two-Dimensional (2-D) e.g films and multilayer sheets.,

1.2.3 Three-Dimensional (3-D) e.g polycrystals etc.,

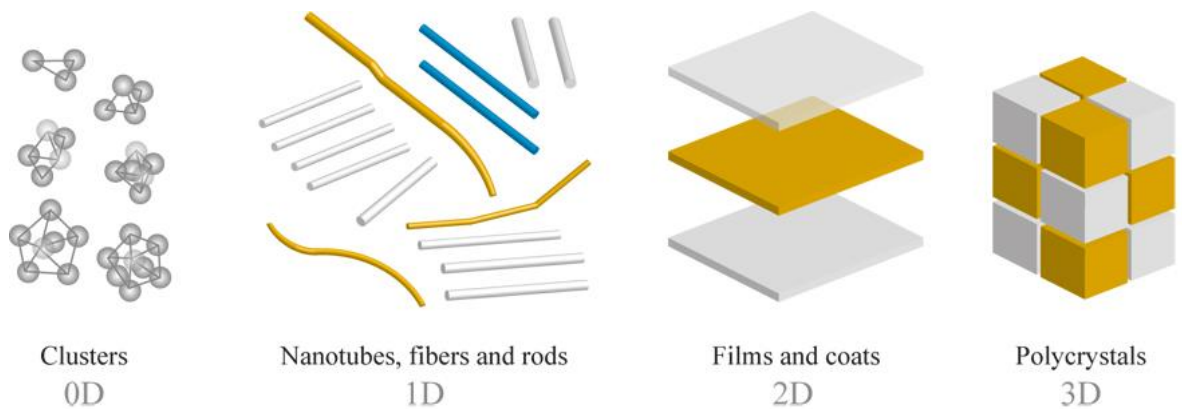


Fig 1.3 Dimensionality of Nanomaterials

The dimensionality of the material is a very important factor because it determines the degree of freedom of charge carriers which profoundly affect many properties of the materials, such as electronic, optical, magnetoelectric, and optoelectrical [14, 16-18].

1.3 Important Concepts of Nanoscience and Nanotechnology

1 inch is equal to approx. 25,000,000 nanometers.

A page of the daily newspaper is approximately 100000 nanometers in width.

If we compare then if marble is a nanometer, then 1 m should be the span of the earth.

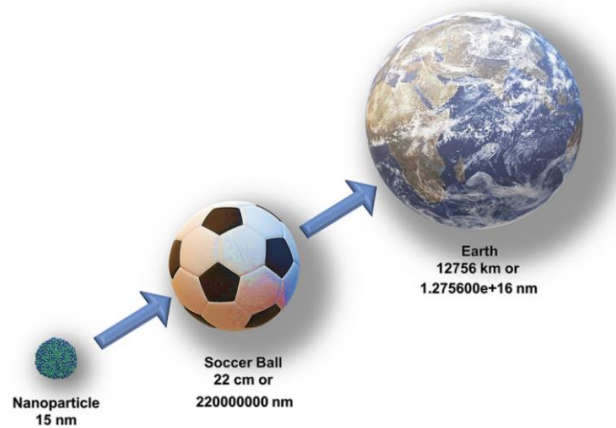


Fig 1.4 Scale of Nanometer (nm)

1.4 Classification of Magnetic Materials

Magnetism and magnetic materials are used in the majority of our electrical and technical gadgets. Transformers, electrical power generators, electrical motors, radio, telephone, television, video system proliferation, and computers are examples of these. Magnetism is the phenomenon in which two materials attract or repel each other due to the movement of electrical charges. It is caused by the orbital and spin movement of electrons.

Magnetic dipoles shift direction in response to an external magnetic field.

According to the Pauli exclusion principle, "no two electrons in an atom can have the same set of four quantum numbers," implying that there would be no magnetic effect if electrons spun in random directions.

Magnetic materials are classified into the following classes based on the response of magnetic dipoles and electrons to an externally induced B-field.

- Diamagnetic
- Paramagnetic
- Ferromagnetic
- Ferrimagnetic
- Anti-ferromagnetic

1.4.1 Diamagnetic Materials

The net magnetic moment of diamagnetic materials with entirely filled atomic orbits is zero. In the opposite direction of the applied magnetic field, an induced magnetic field develops. The shift in electron orbital velocities, which affects the

The magnetic dipole moment is caused by an applied field. The induced dipole moments align themselves in the opposite direction of an applied field. These materials are repelled to the poles of a magnet. Nonmagnetic materials exhibit magnetization in the presence of a magnetic field, indicating the presence of this form of magnetism. Copper, gold, mercury, silver, zinc, and other metals are examples. For these materials, the flux density B is similar to that in vacuum.

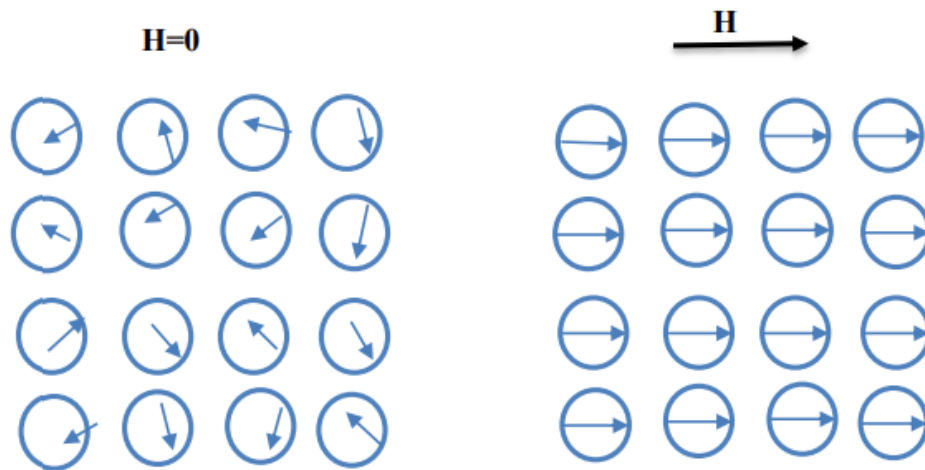


Fig 1.5 Graphical Representation of Diamagnetic Material

1.4.2 Paramagnetic Materials

With no applied field, the partially filled orbitals and unpaired electrons produce a complete magnetic dipole moment. When they are not accompanied by an external field, magnetic moments move in random directions (they do not interact magnetically), and total magnetization is zero. In the presence of a field, the random orientations of moments point in the direction of an external field. Paramagnetic materials are drawn to either pole of a magnet on a weakly basis. This sort of magnetism can be found in nonmagnetic materials such as aluminium, chromium, sodium, titanium, zirconium, and so on. They have the same flux density as diamagnetic materials. As the temperature rises, thermal energy causes magnetic domains to shift.

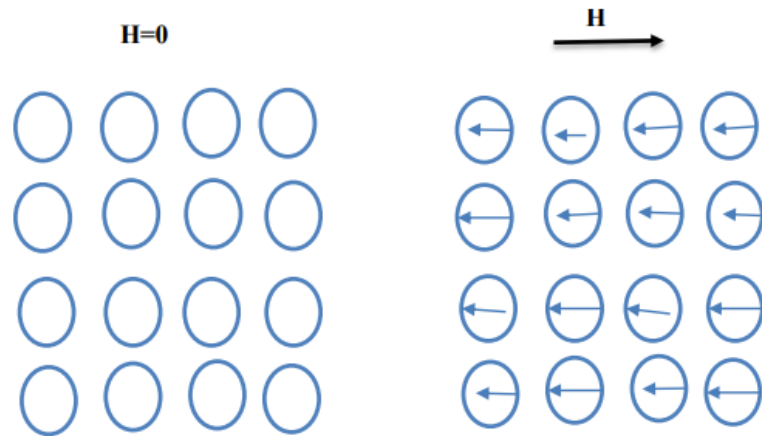


Fig 1.6 Graphical Representation of Paramagnetic Material

1.4.3 Ferromagnetic Material

Even in the absence of a magnetic field, ferromagnetic materials have a persistent magnetic moment. This permanent magnetic moment is derived from atomic magnetic moments caused by uncompensated electron spins. The contribution of orbital magnetic moment is less than that of spin moment. Domains are groups of atoms with aligned dipole moments. In these domains, a large number of moments are aligned in parallel. When there is no magnetic field, magnetic domains are randomly directed, and complete magnetization does not exist. When a magnetic field is present, these domains that are parallel to the orientation of the applied field are referred to as saturation magnetization M_s . This occurs at a temperature of 0 Kelvin. Ferromagnetic materials are drawn to a magnet's poles. These materials' major characteristics are spontaneous magnetization and curie temperature. Cobalt, nickel, iron, and a few rare earth metals, such as gadolinium (Gd), are examples of transition metals that exhibit ferromagnetic properties.

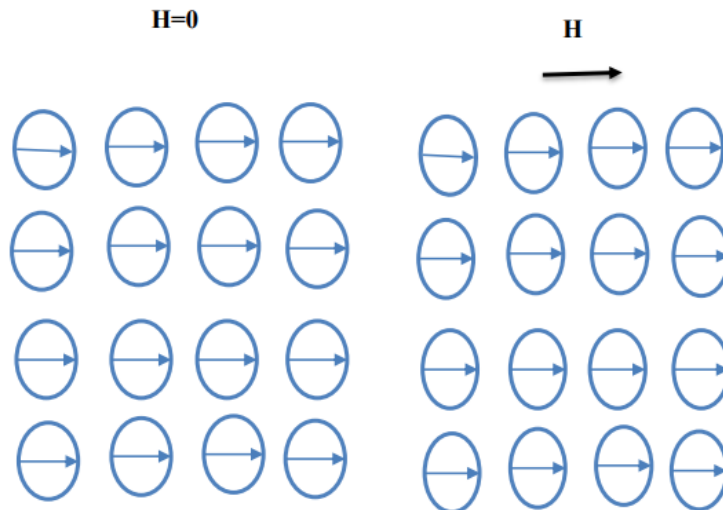


Fig 1.7 Graphical Representation of Ferromagnetic Material

1.4.4 Antiferromagnetic Materials

Because the spin moments of adjacent atoms or ions are oriented in opposite directions, this type of material has no net magnetic moment. At a specific high temperature known as the Neel temperature, these materials behave as paramagnetic materials. Some examples are manganese oxide, nickel oxide, chromium (hematite metal), and iron-manganese (alloy).

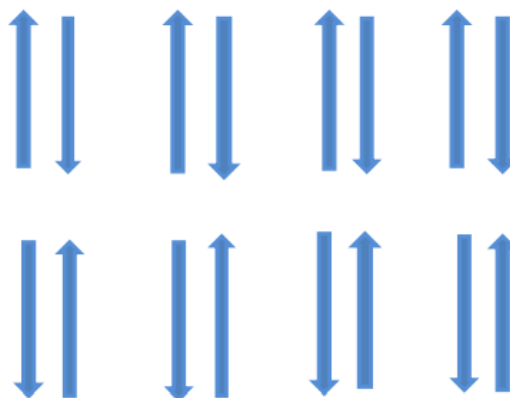


Fig 1.8 Graphical Representation of Antiferromagnetic Material

1.4.5 Ferrimagnetic Materials

These materials, like ferromagnetic materials, have a net magnetic moment. However, with ferrimagnetic materials, the cancellation of spins (parallel and antiparallel) in a domain is partial, resulting in weak magnetism. Ferrimagnetism refers to the

permanent magnetization of certain ceramics. These materials have a lower magnetic permeability than ferromagnetic materials.

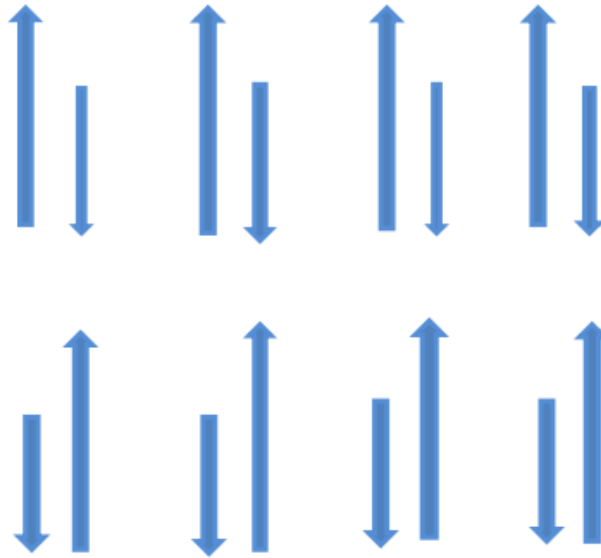


Fig 1.9 Graphical Representation of Ferrimagnetic Material

1.5 Ferrites

A ferrite is a kind of ceramic compound made of iron oxide, an ionic crystal with the chemical formula MFe_2O_4 , where M is a divalent metal cation. Ferrites that are nanoscale in size have shown promise in a variety of fields, including ferrofluids, microwave applications, and magnetic recording medium. The spinel-type ferrite has the benefit of having qualities that can be easily modified and controlled in response to changes in the composition and cation distribution of the material. You can simply alter the attributes to your satisfaction by changing the parameters in the synthesis's preferred path [19-21].

Ferrites are the most essential element used in the production of electronics. They have high permeability and resistivity. Ferrite's saturation magnetization is less than half that of ferromagnetic composites, but it may be applied at higher frequencies, has a high resistivity, is inexpensive, and has excellent heat resistance and corrosion resistance. [22-24].

The major portion of ferrites has a spinel structure and the formula of ferrites:



“A” is the divalent metals, for example, Mg^{2+} , Ni^{2+} , Co^{2+} , Mn^{2+}

“B” is the trivalent atoms, for example, Fe^{3+} and Al^{3+}

The cubic unit cell ferrite contains eight atoms and contains thirty-two O sites and sixty-four T sites. Spinel is fundamentally arranged into an ordinary and opposite spinel. In ordinary spinel, the divalent cations “A” are situated at the tetrahedral side and the trivalent cations “B” on the octahedral side. NiFe_2O_4 and CoFe_2O_4 have opposite spinel structures. In the spinel structure, the A and B are antiferromagnetic. In the opposite spinel “A” cation involves one portion of the octahedral coordination side and a large portion of the “B” cation involves the other half (O) size as well as all “T” side. In spinel structure, the molecule A and a particle B are precisely antiferromagnetic. The turn drops each other. The attractive property ascends because of the 4Fe_2^+ , which adjusts itself on the utilization of the field [25].

1.5.1 Soft Ferrites

This ferrite class is easily magnetised and demagnetized. When combined with a magnetic field, they act as permanent magnets. They can be made by slowly heating and cooling. Soft ferrites include ferrous-nickel alloys, iron-silicon alloys, and garnets. They are employed in the production of electromagnets, computers, transformers, and other data storage devices. Soft ferrites have the following properties:

- Narrow hysteresis loop
- Small coercivity and retentivity
- Low eddy current loss
- No impurities and defects
- Low Magnetostatic energy
- Easier domain wall moment
- Large susceptibility and permeability

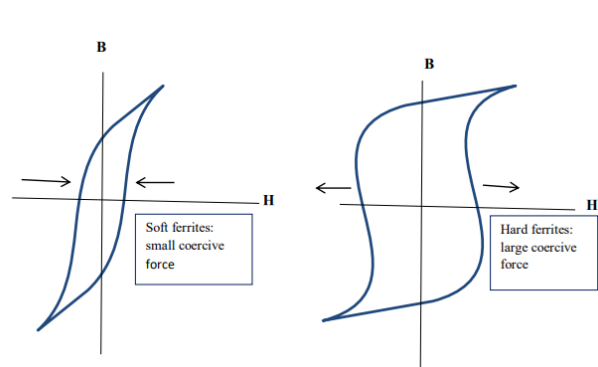


Fig 1.10 Soft vs Hard ferrites

1.5.2 Hard Ferrites

Ferrites in this class are permanent magnets that cannot be easily magnetised or demagnetized. They are created by rapid heating and cooling. They are utilised in the production of permanent magnets and direct current magnets. These ferrites include alnico, iron-nickel-aluminum alloys, chromium, steel, carbon steel, and copper-nickel-cobalt alloys. The following are some of the properties of hard ferrites:

- Wide hysteresis loop
- Large coercivity and retentivity
- High eddy current loss
- impurities and defects are more
- Large Magnetostatic energy
- Difficult domain wall moment
- Small susceptibility and permeability

1.5.3 Comparison of Soft vs Hard Magnetic

Soft magnetic	Hard magnetic
Low Saturation Magnetization	High saturation magnetization
Low Coercivity	High Coercivity
Low Permeability	High Permeability
Low Remanence	High Remanence
Low Curie temperature	High Magnetostriction
Low Magnetostriction	High Curie temperature

1.5.4 Structural Classification of Spinel Ferrites

1.5.4.1 Normal Spinel

Normal spinel structure, in which all Me^{2+} ions occupy A- sites; $Me^{2+}[Fe_2^{3+}]O_4^{2-}$ is the structural formula of such ferrites. This distribution occurs in zinc ferrites $Zn^{2+}[Fe^{2+}Fe^{3+}]O_4$. [21].

1.5.4.2 Inverse Spinel

The structural formula of these ferrites is $\text{Fe}^{3+}[\text{Me}^{2+}\text{Fe}^{3+}] \text{O}_4$, indicating that all Me^{2+} ions are in B-positions and Fe^{3+} ions are equally distributed across A and B-sites. The spinel structure of magnetite Fe_3O_4 , ferrites NiFe_2O_4 and CoFe_2O_4 is inverted. [21].

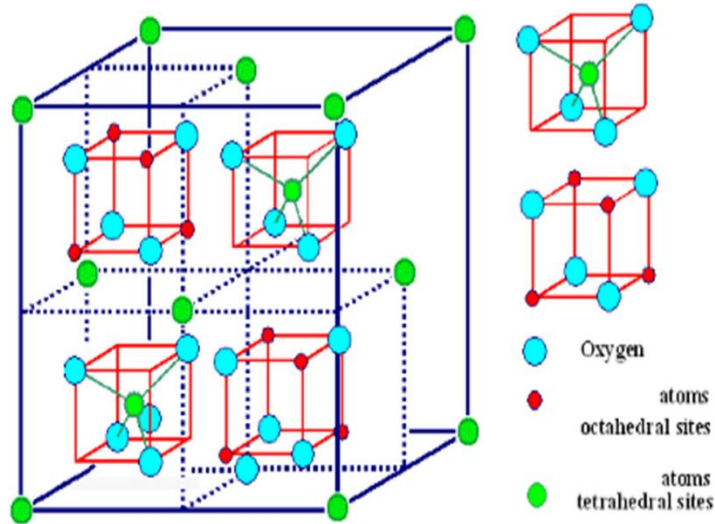


Fig 1.11 Structure of Spinel Ferrites

1.5.5 Why Ferrites?

Most other magnetic materials that are important for technology, such as iron and metallic alloys, have low DC electrical resistance. In light of this, they are not appropriate for higher frequency operations, such as inductor cores in TV circuits. The main issue is that the materials' poor electrical conductivity permits induced current to flow through them, producing heat as a result. Electrical energy is being wasted completely in this, as well as the atmosphere's discharge of it. Materials become extremely inefficient as a result of this energy loss, and this inefficiency increases with frequency. Ferrites, however, have a very high dc electrical resistance, which allows them to function significantly better. The usage of ferrites has expanded because to their significant properties of high permeability and time/temperature stability. They are generally very cheap compare to other magnetic materials [20].

1.5.6 Application of Ferrites

Because of their high electric resistivity, ferrite nanoparticles are highly essential magnetic materials. They have many uses in technology, especially at high frequencies.

Due to the following characteristics, ferrite nanoparticles are commonly employed [19-24].

- Inexpensive
- Mechanical rigidity
- Useful thermodynamic stability
- Microwave frequency usefulness
- Extremely frequent applications
- A variety of materials

1.6 Introduction to Carbon Nanotubes

One of the allotropic forms of carbon, carbon nanotubes contain cylindrical carbon molecules with a length to diameter ratio of roughly 132,000,000:1 [26]. Due to their enhanced heat conduction, electrical, and mechanical properties they are used extensively [27]. The majority of the long, hollow structure of CNTs is composed of one atom thick, chiral rolled graphene sheets.

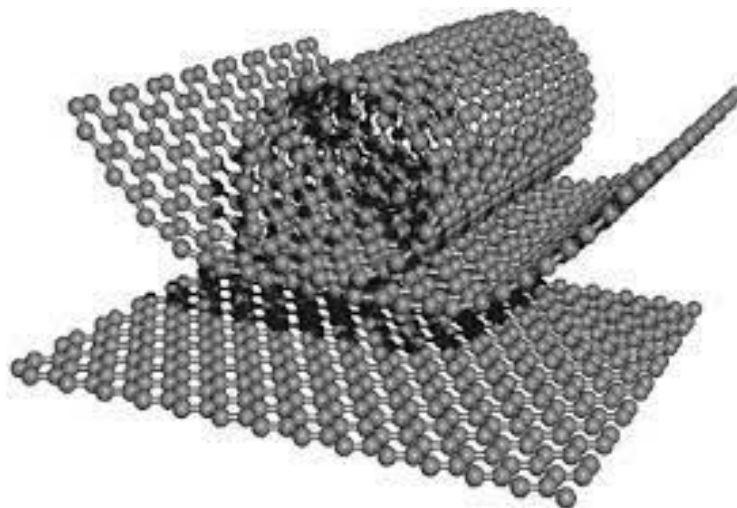


Fig 1.12 Visual Representation of MWCNTs

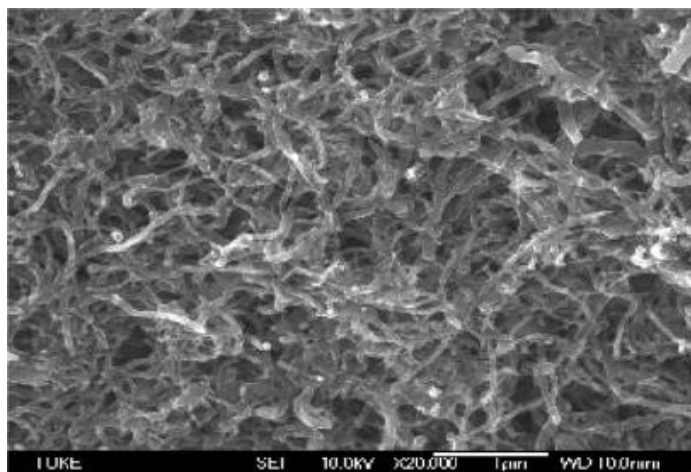


Fig 1.13 SEM Image of MWCNTs

1.6.1 Ferrite/MWCNTs Nanocomposite

Sp² hybridized elemental carbon create the interesting multiwall carbon nanotubes, which are tubular C structures with a honeycomb atomic arrangement (MWCNTs). Due to their exceptional electrical, structural and thermal properties, MWCNTs regarded as useful nanomaterials with a widespread range of potential applications in nanoscience and nanotechnology [28]. MWCNTs adorned with nanoparticles are frequently made utilizing a variety of methods in order to maximize their potential capabilities. Nanocomposites of ferrite/MWCNTs are frequently found to be ideal for dielectric and radio absorption properties. Cobalt ferrite is a well-known inverse spinal hard magnetic material that exhibits remarkable optical electrical and magnetic characteristics [29]. Cobalt ferrite is one of the metal oxide nanoparticles, often known as ferrites, having the chemical composition of MFe₂O₄. (where M could be Co, Ni, Mn, Zn, Fe, etc.). Additionally, CoFe₂O₄ has remarkable chemical stability, resistance to corrosion, and affordability. There are several different chemical processes that may be used to create it. Hydrothermal, hydrogel, microemulsion, solvo-thermal, co-precipitation, etc [30]. There are many potentials uses for the coupling of the two materials, from biomedicine to electromagnetic devices that could be utilized for magnetic data storage, water purification, magnetic force microscopy, and other things. Given the accelerating climatic changes caused by the usage of fossil fuels, we must move from using electricity to produce energy instead of burning them. Even though electric energy is a flexible method of energy, it has a substantial disadvantage. For example, batteries can store enormous amounts of electric power but require a very

long time to charge, making it fairly difficult to store. On the other hand, capacitors charge up instantly but have a limited energy storage capacity. We need to develop a technology that can simultaneously store and discharge vast amounts of electricity for our electrically powered future. One method to do this is to improve a material's dielectric properties [31].

1.7 Objectives of My Project

The following are the goals of this project.

- An affordable and easy chemical co-precipitation approach will be used to create zinc and nickel substituted cobalt ferrite nanoparticles.
- Synthesis of nanocomposites employing toluene as a dispersive technique in a simple one-step ultrasonication assisted process.
- To investigate the effects of MWCNT loading on the electrical and magnetic characteristics of Zinc and Nickel substituted Cobalt Ferrite Nanoparticles.

Chapter 2

Theoretical Review

2.1 Nanoparticles Synthesis Methods

There are two major ways of synthesis of nanoparticles.

- Approach from the top down
- Bottom-up strategy

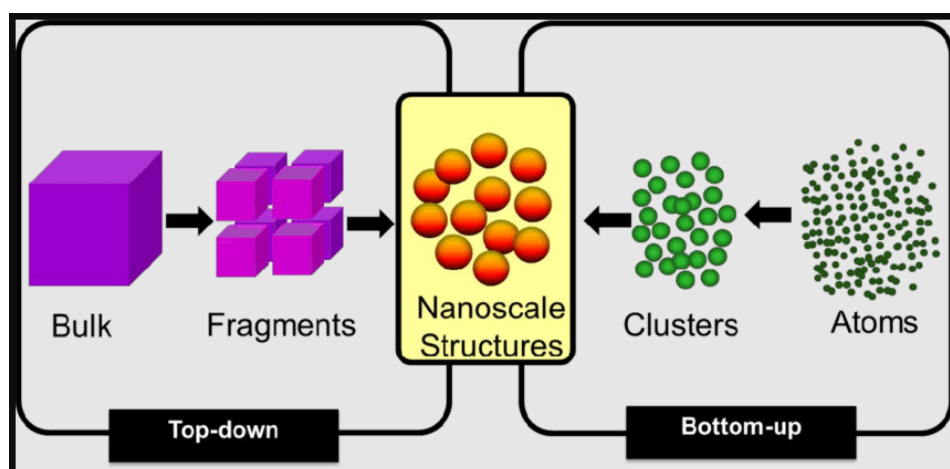


Fig 2.1 Top-Down vs Bottom-Up

2.1.1 Top Down

The top-down technique begins with massive structures and then employs finer technologies, such as lithography, ball milling, laser ablation, electro spinning, arc discharge, and so on, to produce smaller and finer structures.

2.1.2 Bottom Up

To create nanoparticles, the bottom-up technique mixes atoms, molecules, and clusters. Wet chemical synthesis, chemical vapour deposition (CVD), hydrothermal synthesis, physical vapour deposition (PVD), MBE, self-asSEMBly, and other bottom-up approaches are examples.

Both methods have pros and cons. It is difficult to achieve homogeneous nanoparticles of lower size using a top down technique, because a significant amount of impurities is always present. The implementation cost of the bottom up strategy is likely to be

higher. There are various methods for creating nanoparticles. Each method has its own set of benefits and drawbacks. The image below depicts some of the methods.

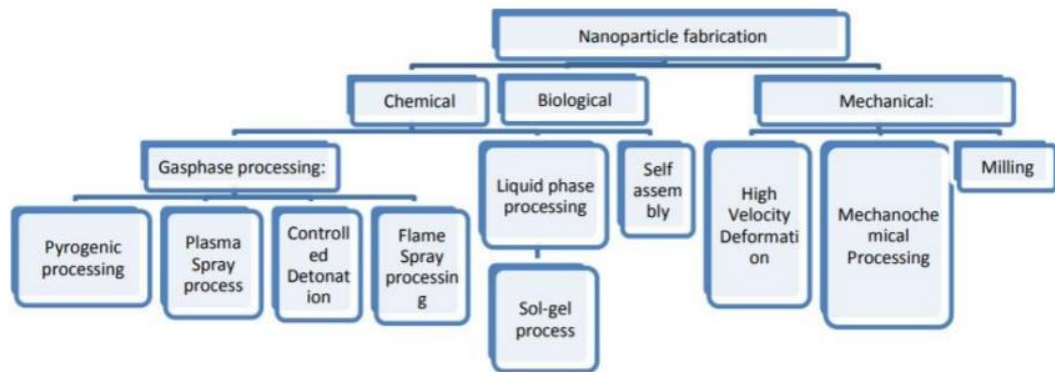


Fig 2.2 Nanoscale Synthesis Methods

Ferrites nanoparticles can be synthesized using a variety of processes, including hydrothermal, solvothermal, coprecipitation, sol gel, micro emulsion, and others. The properties of synthesized ferrite are determined by the synthesis technique and circumstances. A great deal of research has been done and continues to be done on ferrites for diverse uses.

2.2 Some Key Approaches for Producing Oxide Nanoparticles

- Gas Phase Condensation Methods
- Microwave Plasma Processing
- Hydrothermal Synthesis
- Electric Dispersion Reaction
- Combustion Synthesis
- Sol-Gel (Colloidal) Processing
- Sonochemical Processing
- Spray Pyrolysis
- Chemical coprecipitation method
- Mechanochemical Synthesis

2.2.1 Gas Phase Condensation Methods

Aerosol processing is commonly used to create nanoparticles from gas condensation of precursor molecules. The first step is to generate gaseous precursor molecules using

a suitable physical or chemical approach. The precursor molecules then react in the gas phase to generate nuclei of the chosen phase. A typical nucleus has dimensions comparable to a refractory oxide. The approach is suited for both laboratory and industrial-scale nanoparticle manufacturing. Time, temperature, and the number of particles produced per unit volume are all essential aspects in the gas phase condensation process. Various methods are employed in the gas phase condensation of oxide nanoparticles.

2.2.2 Microwave Plasma Processing

The approach is appealing for overcoming the kinetic and thermodynamic obstacles found in traditional solid-state synthesis. The faster rate in the process is due to the reactants being exposed to microwave rather than conventional furnace heating. To prepare nanophase oxide powders, the precursor can be a homogenous solution or a gaseous precursor. The chemical created as a result of energy transfer in the plasma between electrons and other species. The energy transfer between electrons and species present in the plasma is determined by the frequency of the source and the number of collisions. Some binary oxides have been prepared using this technique.

2.2.3 Hydrothermal Synthesis

Hydrothermal synthesis generates fine powders of advanced ceramic oxides by utilising the characteristics of water under high pressure and temperature. With a pressure of up to 15 MPa, the reaction temperature is between the boiling point of water and the critical temperature of 374° C. The benefit of employing the hydrothermal process is that the final product is formed without calcination and has fine crystallite with superior morphological control, content, purity, and powder reactivity. The precursor is made from metal nitrates, oxides, and hydroxides and is subjected to high pressure in a specially built hydrothermal bomb (autoclave). The process is based on increasing precursor solubility in water under hydrothermal conditions, which ensures the development of a homogenous and well-controlled final product.

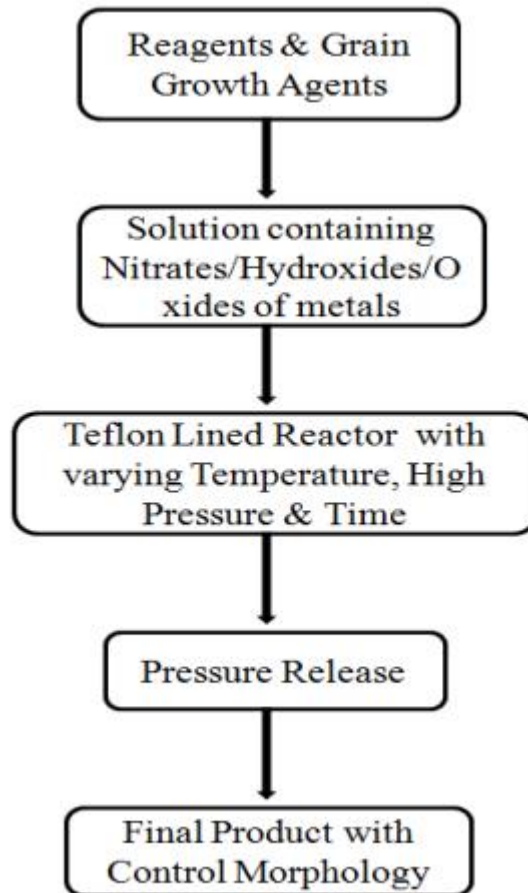


Fig 2.3 Flowchart of Hydrothermal Method

The hydrothermal approach was discovered to be successful in the manufacture of nanoscale ceramic oxides and a variety of new materials. The hydrothermal process is useful for producing electrical and dielectric ceramic powders with better properties. For the production of nanoparticles, the hydrothermal approach can be coupled with other techniques such as hydrothermal-sonochemical and hydrothermal-microwave processing.

2.2.4 Electric Dispersion Reaction

Electric dispersion is a precipitation reaction that occurs in the presence of a pulsed electric field in order to produce ultrafine precursors of advanced ceramic materials. The sole is broken into micron-size droplets bearing hydrous precursor precipitates under the applied electric field (3 to 10 kV/cm at a pulse frequency of 1 to 3 kHz), which can then be thermally treated to obtain oxide nanoparticles.

2.2.5 Sol-Gel (Colloidal) Processing

Sol-gel is a popular method to prepare wide variety of oxides in different shapes (particles, films, fibers, etc.). The sol is formed by mixing the metal salt precursors (organic, inorganic or alkoxide) in a suitable solvent. The polymeric network is formed upon drying the sol, in which solvent molecules are trapped inside solid gel.

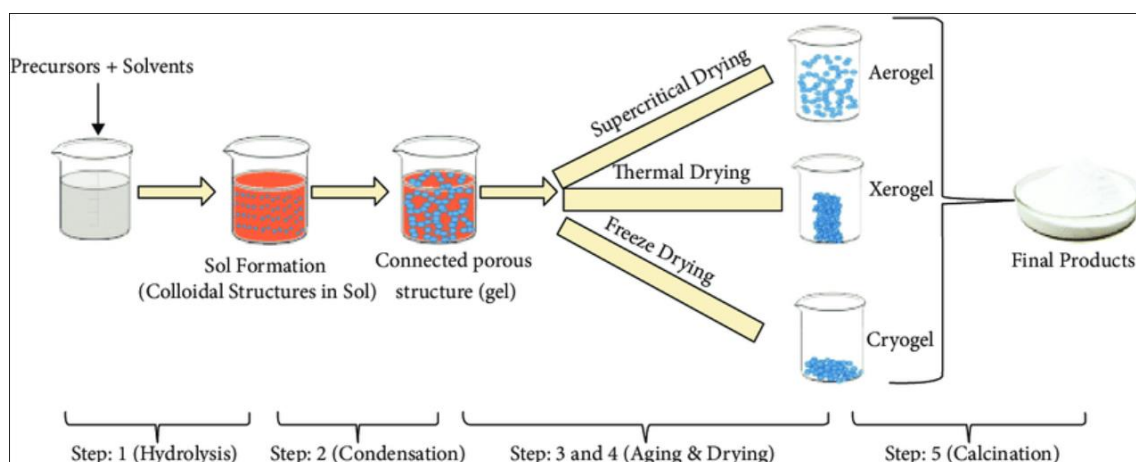


Fig 2.4 Use of Sol-Gel Technique in Synthesis of Various products

The final ceramic oxide is formed as a result of the subsequent heat treatment Fig 2.4. The sol gel approach uses atomic scale synthesis, which reduces diffusion distance as compared to the solid-state reaction method and allows for the formation of products at considerably lower temperatures. The intermediate species involved in the sol-gel process are determined by the type of the precursor, which can be an aqueous solution of metal organic or inorganic salt. Solution oxidation, concentration, and pH are all important elements in colloidal formation and stability. The chemical manipulation of the precursor sol and the nature of the generated colloid have a significant impact on the qualities of the end product.

2.2.6 Sonochemical Processing

The application of ultrasounds in chemical synthesis has ushered in a new era of processing technologies. The material's sol is subjected to high intensity ultra sound (50 to 500 W/cm²) and extreme acoustic circumstances, which compel the reactants to overcome the activation energy barrier in a very short time to create the final phase. Interparticle shape, reactivity, and composition change as a result of ultrasonic agitation. The shape of oxide nanoparticles is influenced by the type of surfactant and the concentration of the sol. Sonochemical methods have been discovered to be

beneficial for the development of mesoporous materials that can be utilised to eliminate harmful organic compounds from the environment.

2.2.7 Spray Pyrolysis

Spray pyrolysis is frequently employed for the creation of ultrafine particles and thin films with commercial scale potential. Metal ions are suspended in a gaseous environment after being sprayed through a nozzle. The suspended droplets are thermally treated until they reach the final phase. Spray pyrolysis varies due to different thermal treatments. Because of its simplicity and capacity to synthesize complicated multi-component oxides, spray pyrolysis is preferable to gas phase condensation. Spray pyrolysis produces less agglomerated and higher crystallinity products than sol-gel and precipitation processes. Spray pyrolysis makes it difficult to manage particle shape.

2.2.8 Combustion Synthesis

Exothermic reactions are used in the combustion process to surpass the activation energy barrier for product production. The precursor is a redox combination of reducing organic compounds and oxidising metal salts. As the temperature rises to the ignition point of the fuel, the mixture burns in a self-propagating manner. This is a quick process that requires little input energy while producing a wide range of ceramic oxides. The rate of reaction is determined by the amount of fuel in the initial mixture. The optimal fuel concentration should be chosen to create high surface area nanoparticles with sizes ranging from 10 to 20 nm.

2.2.9 Mechanochemical Synthesis

Mechanical milling over time is a low-cost commercial manufacturing method for nanoparticle creation. During the milling process, the rate of reaction and production is determined by the high energy of impact velocity and frequency. Long-term milling of reactive components reduces their size and increases surface area, increasing reactant diffusion. When compared to conventional solid state synthesis, high energy milling yields crystalline phase at much lower temperatures. The method has been used to a wide range of oxide nanoparticles. The main disadvantage of the

mechanochemical approach is the introduction of strain, contaminations, and the extended reaction time.

2.3 Chemical Co-Precipitation Method

A common synthesis method that is frequently cited in the literature is co-precipitation. Massart was the one who initially suggested this technique, and the following equation used to describe the chemical process that takes place.

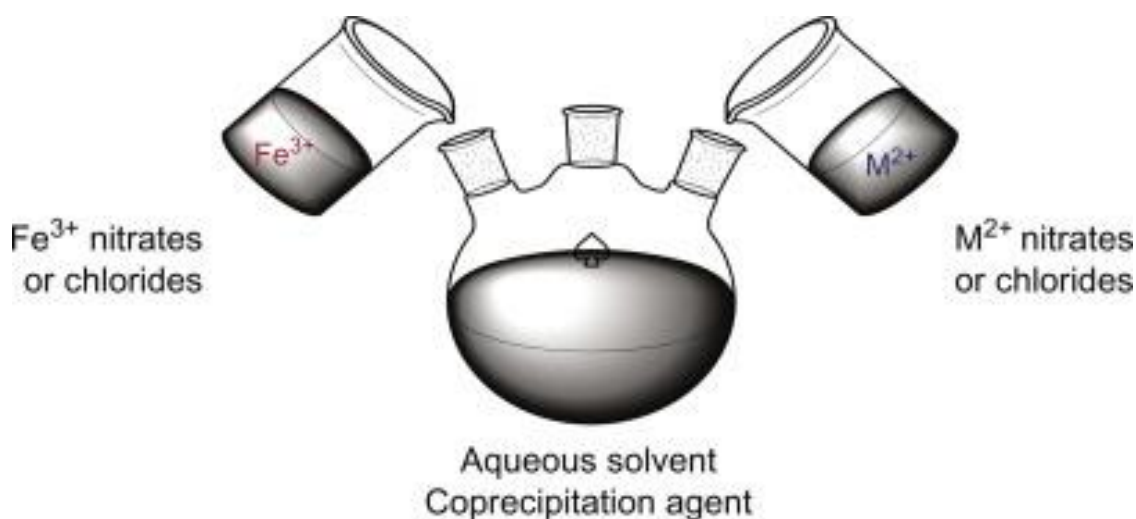
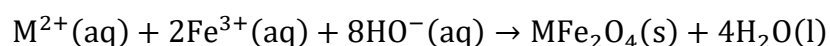


Fig 2.5 Visual Representation of Co-Precipitation Reaction

This approach is still constrained by a few issues, such as the ability to manage particle size and form, crystallinity, and magnetic characteristics. In order to fine-tune the size, shape, and chemical makeup of the obtained NPs, it is crucial to research and control the reaction parameters (such as the type of metal cation precursors, the molar ratio among M(II) and Fe(III) cations, temperature during reaction, pH value, and type/concentration of alkaline agent). The results of several research have discussed the effects of changing these factors.

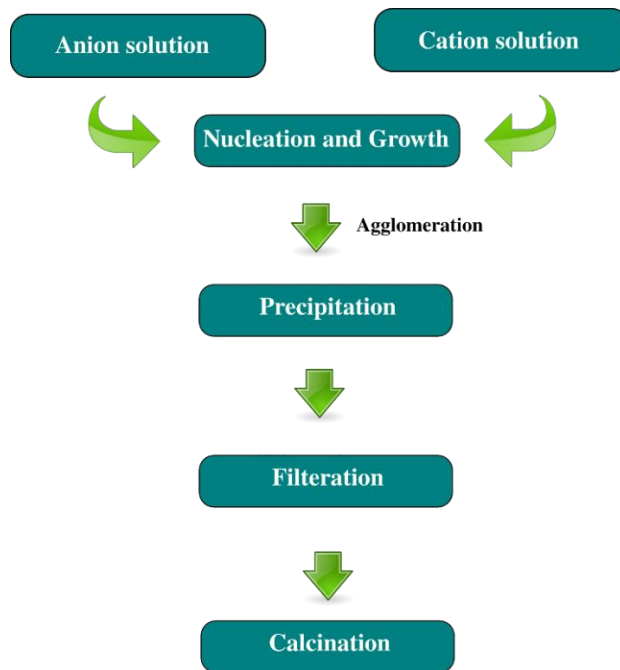


Fig 2.6 Flow Chart of Co-Precipitation Reaction

2.3.1 Why Co-Precipitation Method

It is highlighted as a straightforward, affordable, and quick approach that may be rapidly expanded for industrial applications. It provides a nanomaterial with excellent purity by an eco-friendly approach, without needing treatments under high temperature or pressure nor toxic organic solvents. The co-precipitation strategy has the advantage of creating nanocrystals that are smaller than generated by conventional synthesis processes, depends on the catalyst used during the reaction. Additionally, by adding capping agents, the size and shape of the crystallites in the material produced using this process may be regulated. However, the co-precipitation process has some significant drawbacks, including the need for constant washing, drying, and calcination to produce a pure phase of required nanoparticles [32] [33].

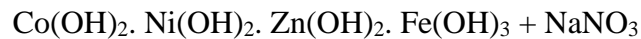
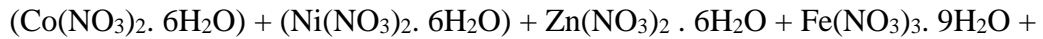
2.3.2 Steps in Co-precipitation

Co-precipitation involves two major steps:

1. Co-precipitation step
2. Ferritisation step

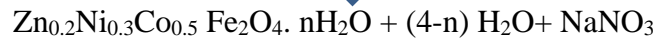
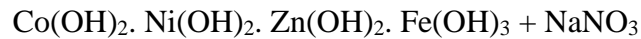
2.3.2.1 Co-precipitation Step

The co-precipitation of metal cations in alkaline solution results in metal hydroxides in the form of colloidal particles. The reaction occurs in the case of Zn-Ni-Co ferrites:



2.3.2.2 Ferritisation Step

The product is heated in an alkaline precipitation solution to convert the metal hydroxides solution to Ni-Zn ferrites.



Washing the product with deionized water until the pH value reaches neutral removes the ionic contaminants of Na and NO₃.

2.3.3 Parameters Involved in Co-Precipitation:

Parameters with influence on the co-precipitation process are described below:

- Rate of mixing of the reactants
- Role of anion
- Temperature effect
- Effect of pH
- Heating after co-precipitation

2.3.3.1 Rate of Mixing of The Reactants

The rate of mixing greatly influenced the size of the particles. If the growth rate is slow and the nucleation rate is higher than the growth rate, then small size of the particles is achieved and vice versa. In first case the rate of mixing of the precursors is very high and in the second case rate of mixing is low. Slow mixing gives the particles of homogeneous chemistry.

2.3.3.2 Role of Anion

Anions can exist in the form of metal ion solutions or salts. The usage of metal salts is recommended for optimum results. Sulphates, nitrates, and chlorides are the metal salts utilised in Co-precipitation. These salts are chosen for their ability to be easily removed from the finished product, typically through washing or decomposition during the heat treatment process. Because of their propensity to easily leave the metal ion, nitrates and carbonates salts are commonly utilised as metal precursors. As a precipitating agent, it is used with ammonia or sodium carbonate. Chloride and sulphates are poisonous ions that should be avoided since they impede the creation of high purity particles.

2.3.3.3 Temperature Effect

Varying metals require different amounts of activation energy to make ferrites. The activation energy is provided by the heat energy provided to the reactants. The reaction temperature is controlled between 70 and 100 degrees Celsius during the synthesis of nickel-zinc ferrites. This temperature range is critical for determining crystallite size and, as a result, the surface area of the particles generated. Researchers have found it difficult to pinpoint the exact influence of precipitation temperature, with results ranging widely; however, it has always been discovered that nucleation rates are temperature dependent.

This can be attributed to the process's kinetics and the activation energies of the chemicals in the reaction solution. Some research indicate that temperature controls the nucleation process, while others demonstrate an enhanced rate of growth and coarsening.

2.3.3.4 Effect of pH

PH is important in the production of particles with regulated size and shape. Because the pH of a reaction system influences the degree of super saturation of the nanoparticles in the reaction solution, it is believed to have a significant impact on the final properties of the nanoparticles generated. There is, however, no general rule of thumb, and the influence of pH on each reaction is unique and must be researched for each system.

In the Zinc oxide thin film deposition system, for example, a film formed below the pH value of 8 is porous and almost opaque, whereas a film formed above the pH value of 13 is milky white and almost defect-free; however, studies have shown that the best results were obtained at pH values between 11 and 13. This is related to the shift in phase formation as well as the effect of pH on reaction kinematics. Significant particle development is not possible at low pH levels. Increasing the pH value; the particle's growth rate is sufficient. A reduction in the pH value reduces the time necessary for product production.

2.3.3.5 Heating After Co-Precipitation

Annealing is essential to obtain the desired final product phase. The temperature and duration of heating are critical because they influence the size and shape of the particles.

Chemical co-precipitation has numerous advantages over other synthesis methods.

- Formation of monodispersed and homogeneous particles
- Particle preparation that is quick and easy
- Particle form and size are freely adjustable.
- Particle composition can also be modified.

2.4 Synthesis of Zn-Ni Substituted Co ferrite/MWCNTs Nanocomposite

To make the Zn-Ni substituted Co ferrite and MWCNTs nanocomposite, pre-acquired MWCNTs and annealed Zn-Ni substituted cobalt ferrite nanoparticles obtained after co-precipitation were mixed in 200ml of toluene and sonicated for several hours at room temperature for uniform dispersion. Dropwise addition of uniformly distributed ferrite particles in toluene medium to MWCNTs dispersion was then performed, and the resulting mixture was sonicated for 12 hours using a water bath ultrasonicator. To avoid agglomeration, the carrier toluene fluid evaporated, leaving behind an evenly dispersed nanocomposite that was further homogenised by mechanical mixing (solid state technique). In order to assess the increased loading effect of MWCNTs on magnetic, electrical, and dielectric properties of the produced composite, the weight percentage of MWCNTs was continually altered (0%, 0.25%, 0.5%, 0.75%, 1%)

2.5 Toluene as a Dispersion Medium

Toluene, often known as toluol, is an aromatic substituted hydrocarbon. It is a colourless, water-insoluble liquid with the odour of paint thinners. It is a benzene derivative with a methyl group connected to a phenyl group that is monosubstituted.

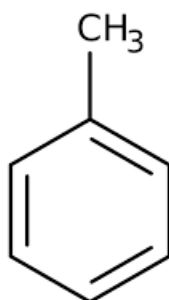


Fig 2.7 Toluene Chemical Structure

The density of each isomer is 0.867g/mL, which is lower than that of water, making toluene a viable choice for dispersion. Because toluene has a benzene ring structure, which requires electron sharing between the six carbon atoms in the ring, other electrons within the molecule's bonds are drawn to the ring structure. Because cobalt has a tendency to give up electrons, achieving a valence state of (Co⁺²,Co⁺³), and iron has a tendency to give up electrons, achieving a valence state of (Fe⁺²,Fe⁺³), a weak polarisation or Van Der Waals forces are formed, resulting in complete mixing and dispersion of MWCNTs and Ferrite particles.

Chapter 3

Methodology

3.1 Material and Apparatus

3.1.1 Chemical Used

The following compounds were utilized throughout the $Zn_{0.2}Ni_{0.3}Co_{0.5}Fe_2O_4$ and MWCNT nanocomposite synthesis without additional purification.

- a) Analytical grade nitrates of Fe (Duksan), Co (Merch), Zn (AppliChem), and Ni (Sigma-Aldrich).
- b) Analytical grade Sodium Hydroxide (Sigma-Aldrich).
- c) Analytical grade pristine Multiwalled carbon nanotubes.
- d) De-ionized water from TKA smart2pure system.

3.1.2 Apparatus Used

Glassware	Class A, Pyrex, Ceramic crucibles
Oven	Memmert, Model 500, 108 lit
Heating Stir stirrer	Stuart heat stirs CB162; ARE heating magnetic
Hydraulic Press	Specac, 0 to 15 tons
FTIR Spectrometer	PerkinElmer, Spectrum 100, FT-IR
Furnace	Muffle furnace by PCSIR
XRD	D2 phaser by BRUKER
SEM Ion	JSM-6490 Scanning Electron Microscope; 1500

sputtering Device

Resistivity Measurement In-house built two probe apparatus, KEITHLEY
6487PICOAMMETER/Voltage Source

Dielectric Measurement WAYNE KERR Precision Impedance Analyzer
6500B

3.2 Co-Precipitation

Separate solutions of nitrates of Co, Ni, Zn, and Fe in the requisite concentrations were produced in de-ionized water. These solutions were combined and agitated for 10 minutes before being heated to 90°C with NaOH to control the pH to about 11-12 for the co-precipitation of metal hydroxide to occur, which is then subsequently neutralized by washing the sample with de-ionized water. The respective composition was made using the simple stoichiometric formula.

$$Mass = \frac{Molarity \times molecular\ mass \times 200\ ml}{1000}$$

Aqueous solutions having molarities of 0.2 of Iron Nitrate(III) Nonahydrate ($Fe(NO_3)_3 \cdot 9H_2O$), 0.05 of Cobalt Nitrate (II) Hexahydrate ($Co(NO_3)_2 \cdot 6H_2O$), 0.02 of Zinc Nitrate $Zn(NO_3)_2 \cdot 6H_2O$ and 0.03 of Nickel Nitrate $Ni(NO_3)_2 \cdot 6H_2O$ were taken in deionized water and mixed with one another at ambient temperature while stirred them for approximately 20 minutes. We heat them up to 90°C while stirring constantly, and an aqueous solution of sodium hydroxide with a molarity of 3 M was taken and heated to 90°C while stirring constantly. The sodium hydroxide aqueous solution was then added to the aqueous solutions of iron nitrate, cobalt nitrate, Zinc nitrate and nickel nitrate salts. For an hour at 90°C, the solution was constantly stirred. The products were eventually cooled to room temperature and washed with double distilled water numerous times to obtain free of impurity cobalt ferrite particles as precipitates associated with a small amount of water that were eliminated, and dried powders of cobalt ferrite nanoparticles were obtained by heating for a long time at 100°C in the oven.

3.2.1 Sample Processing

The powders were calcined at 800°C in a muffle furnace for three hours to remove carbonaceous impurities and achieve a distinct phase of spinel. To avoid agglomeration, the powder was ground with a mortar and pestle.

3.3 Study of Synthesized Samples

- a) X-Ray diffraction
- b) Fourier transform infrared spectroscopy
- c) Scanning electron microscopy
- d) EDS
- e) DC electrical resistivity measurement
- f) Dielectric properties measurement

3.4 X-Ray Diffractions

X-Ray diffraction is common technique for material analysis. They can be used to examine thin films as well. The features of the materials are displayed in the x-ray diffraction spectra. The XRD displays the material's crystal phases. The XRD displays the material's crystallographic orientation. We can identify a variety of structural characteristics, including material strain, grain size, crystal lattice parameter, the makeup of the phases that are present in the material. We can determine the thickness of thin films and several layers using x-ray diffraction. Only crystalline materials can be used for X-ray diffraction. Atoms are arranged in arrays in crystalline materials. X-rays can be thought of as electromagnetic radiation waves. Crystals' organized atoms scatter incident x-rays mostly through their electrons. Elastic scattering is the term for this phenomenon. Atomic electrons perform the function of an electron scatterer. Due to their differing orientations, the majority of these waves cancel each other out and generate destructive interference.

The diffraction plane spacing, incident angle, integer n , and wavelength of the incident x-ray are all included in the formula for Bragg's law. Copper K-alpha is typically employed as an x-ray source. 8.04 keV is the same as the energy. The x-rays employed in XRD have a wavelength of 1.5406 Å .

3.4.1 Basic Principle of X-Ray Diffraction

The X-Ray beam strikes the sample and crystal planes, which act as mirrors, and the angle of their reflection equals the angle of incidence, also known as constructive interference. The interference of x-rays within the crystal is caused by the interference of each set of atoms. Interference can be characterized by Bragg's Law, which is provided by:

$$n \lambda = 2d \sin \theta$$

Where, λ =wavelength of the ray

n = integer (1, 2, 3,)

θ = angle between incident ray and surface of crystal

d = spacing between the layers of atom

Constructive interface occurs when n is integer (whole number)

According to Bragg's law, radiations are reflected from a path difference of $2d\sin\theta$ that is subjected to evenly spaced planes at a distance of ' d ' and " θ " is measured from plane. As seen in Fig 3.1, constructive interference can be created. Reflection can only occur in the above-mentioned equation when $\lambda < 2d$, which is why visible light cannot be used.

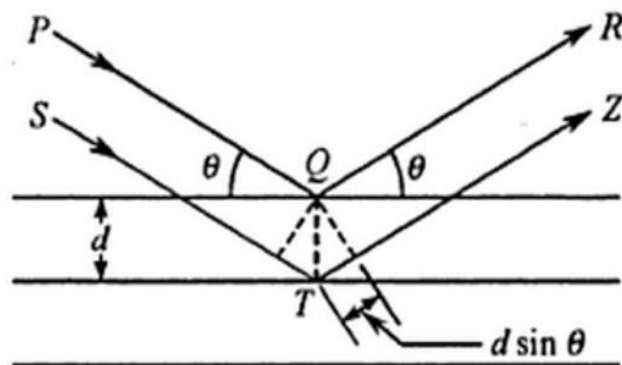


Fig 3.1 Bragg's Law Reflection as The Constructive Wave Interacts

3.4.2 Different XRD Approaches

For XRD characterization, three approaches are typically utilized.

- The Laue technique
- Rotating crystal technique
- Powder diffraction technique

3.4.3 Powder Diffraction Method

We employ the powder diffraction method since the prepared sample is made up of nanopowder. When single crystals of adequate sizes are unavailable, this approach is best suited. The prepared sample powder is coarsely ground to a tiny size and then placed in a circular plate of aluminum or glass for this approach. The X-rays strike prepared powder that is randomly oriented in relation to the X-rays. The formation of a diffracted cone of radiation in the powder approach is depicted in Fig 3.4. Some of the nanoparticles are oriented in such a way that their (hkl) planes produce the optimal Bragg angle for a specific reflection.

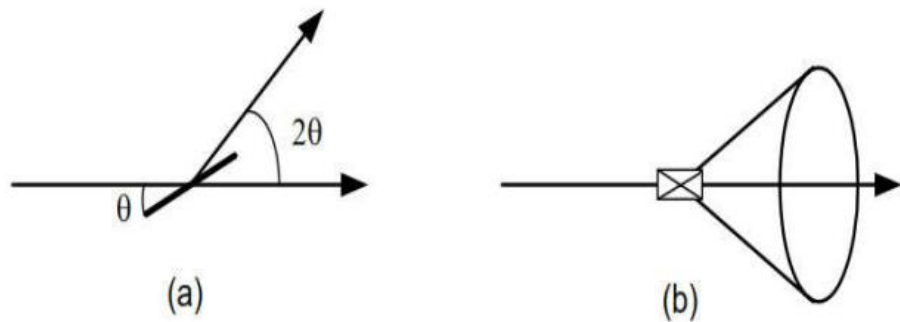


Fig 3.2 Formation of Diffracted Cone

3.4.4 X-Rays Generation Explanation

The underlying explanation for the generation of x-rays is thermionic emission. High energy electrons created by heating a tungsten filament (copper cathode) are accelerated by high voltage and allowed to fall on a target material in x-ray generation (anode). Upon striking the anode, if incident electrons are suddenly decelerated; x-rays produced in these events are called "braking radiations" or "bremsstrahlung radiations". The inner shell electrons of the target material are knocked out by incoming electrons with sufficient energy. Upper shell electrons fill such voids, releasing x-rays of energy specified by the electron's energy levels.

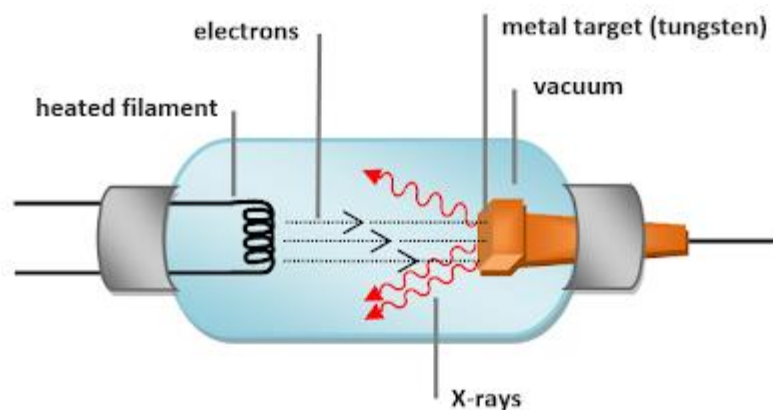


Fig 3.3 Visual Representation of Production of X-Rays

3.5 Fourier Transform Infrared Spectroscopy (FTIR)

Fourier transform infrared spectroscopy is known as FTIR. It also well known as FTIR spectroscopy and analysis. Materials that are polymeric, organic, or inorganic can all be identified using FTIR. The FTIR device has a special method for classifying compounds. A sample is exposed to infrared radiation from 10,000 to 100 cm^{-1} , part of which is absorbed by the sample. The molecules in the sample convert the radiation that is received into rotational and vibrational energy. At the detector, the follow-on signal appears as a spectrum, primarily between 4000 cm^{-1} and 400 cm^{-1} . Because every molecule or chemical structure will produce a different spectral fingerprint, this represents the sample's chemical fingerprint [34].

Using a Perkin-Elmer Spectrum 100 FT-IR Spectrometer at room temperature, the samples' FT-IR spectra are captured across the wavelength range of 380 to 1000 μm . Using FT-IR in the wave number range of 380 to 1000 cm^{-1} , the vibrational modes of the octahedral and tetrahedral metal complex in the sample have been examined. It reveals an absorbing band within this range, confirming the spinel structure of the sample.

3.5.1 What Information Can FT-IR Provide?

It is capable of identifying unknown materials; determining the quality or uniformity of a sample; and determining the quantity of molecules in a combination.

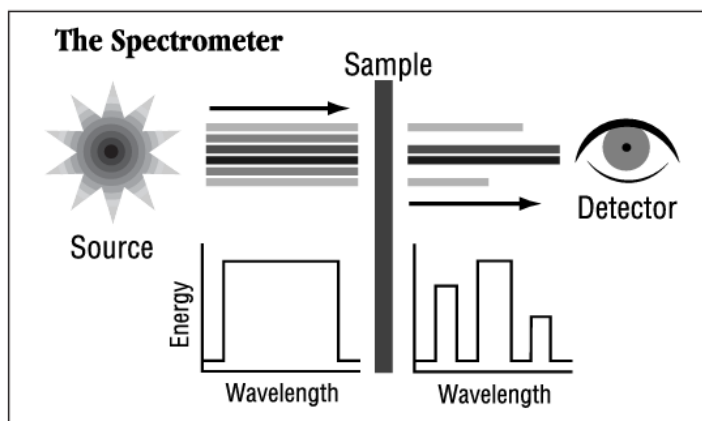


Fig 3.4 Working Principle of FTIR

Radiation from the source causes the sample to go through the interferometer and end up at the detector. The signal is then amplified and transformed into a digital signal by an analog-to-digital converter and an amplifier, respectively. The signal is eventually sent to a computer, where the Fourier transform is run. An FTIR spectrometer's block diagram is shown in Fig 3.4.

3.5.2 FTIR Sample Preparation

Because alkali salts have no absorption in the IR spectrum, the sample was prepared using the KBr pellet method. The die was filled with a mixture of KBr and sample before being placed in a hydraulic press system at 3 tones for nearly 15 seconds. After 15 seconds, the pressure was released, and the die was extracted. Finally, a thin sample pellet with a thickness of 2-3 mm and a diameter of 13 mm was obtained and used for FTIR testing.

3.6 Scanning Electron Microscope (SEM)

SEM stands for scanning electron microscope. The SEM is a type of microscope that uses electrons rather than light to produce pictures. Since its creation in the early 1950s, SEM has resulted in the creation of new research fields in medical and physical

science. Scientists can now examine a much broader range of specimens thanks to the SEM. [35].

3.6.1 How SEM Works

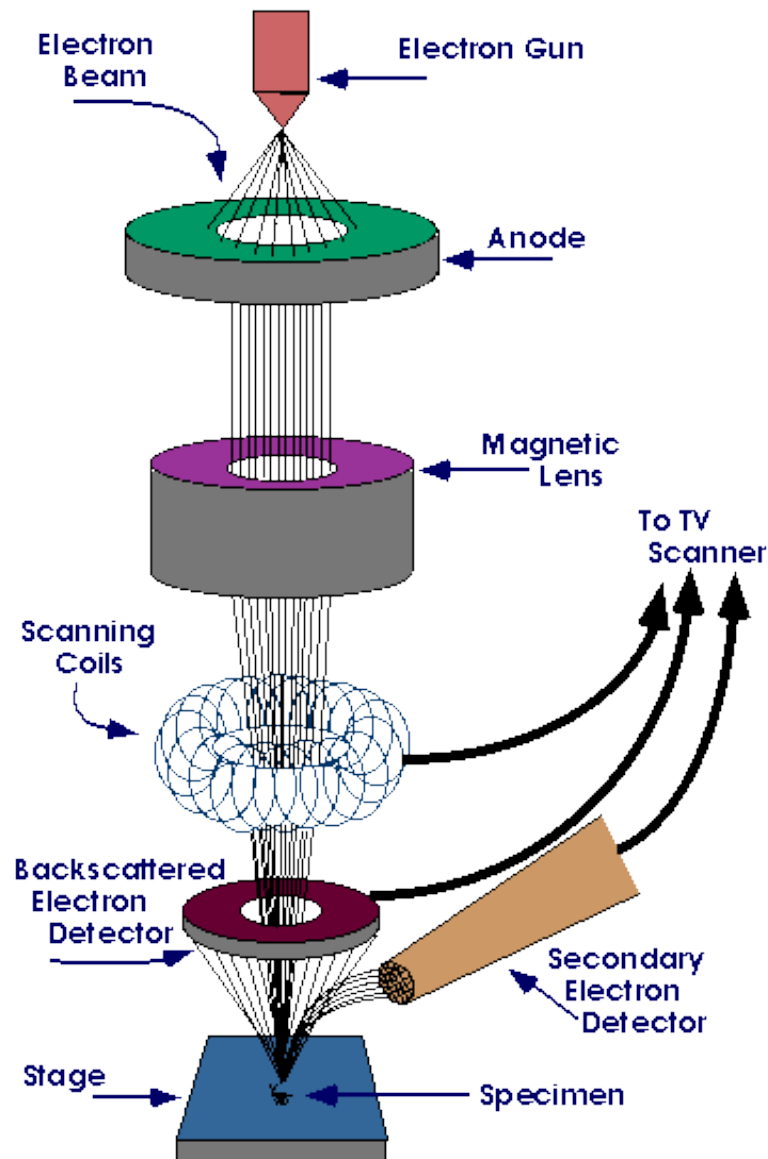


Fig 3.5 Principle of SEM

The SEM is a device that forms a picture using electrons rather than light, resulting in a significantly enlarged image. An electron cannon at the head of the instrument produces an electron beam. The microscope is maintained in a vacuum and the electron beam travels through it in a vertical direction. The beam is focused downward toward the sample as it passes via electromagnetic fields and lenses. Electrons as well as X-rays are expelled from the sample once the beam strikes it [36]. These secondary

electrons, backscattered electrons, and X-rays are collected by detectors, which then turn them into a packet that is transmitted to a display like to a television. The result is the finished picture [37, 38].

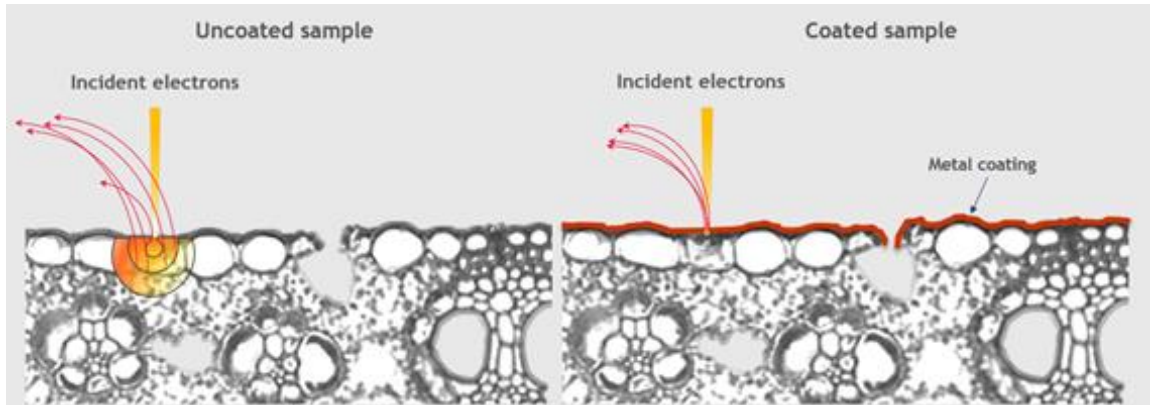


Fig 3.6 Illustration of Electrons and Matter Interaction with Coated vs Uncoated Sample

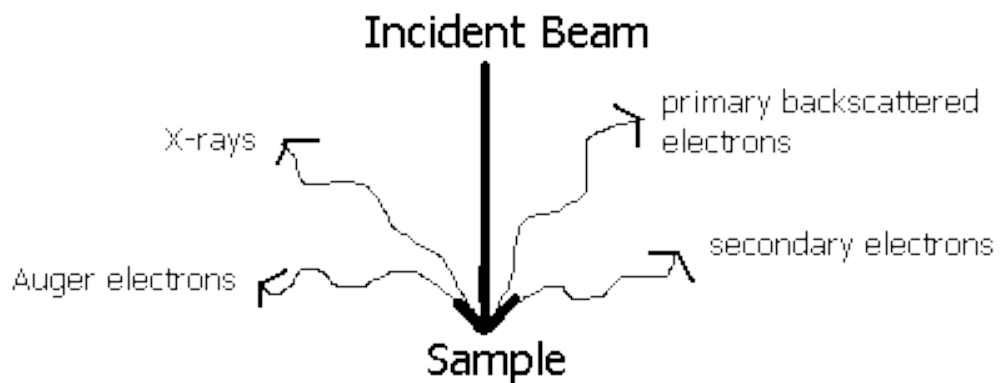


Fig 3.7 Interaction of Incident Beam and Sample

3.6.2 Precautions of SEM

The primary requirement for taking images of samples using a scanning electron microscope is that the sample be conducting in nature. When employing metallic or conducting materials, no problems exist; nevertheless, insulators cause problems. A thin film of gold or palladium is deposited over the sample to conduct it in order to acquire clear photographs of insulators. Chemically treated items must be carefully washed and dried to minimize structural damage due to surface tension.

3.6.3 SEM Sample Preparation

SEM is useful for obtaining a three-dimensional image of the surface and seeing huge items. A little amount of powdered material was mixed with toluene and sonicated for 2 hours. The mixture was poured onto a clean glass slide and dried in an oven for an hour before being utilized for SEM/EDS analysis.

3.7 Vibrating Sample Magnetometer (VSM)

Simon Foner created the first vibrating sample magnetometer at Lincoln Laboratories in 1959. His primary goal is to test the routine magnetic properties of magnetic materials such as ferrimagnetic, ferromagnetic, antiferromagnetic, diamagnetic, and paramagnetic at various temperatures.

3.7.1 Mechanism of VSM

The mechanism of a vibrating sample magnetometer is based on Faraday's law of induction, which states that a homogeneous magnetic field is applied to the sample and vibrated at a modest, fixed amplitude. In relation to the vibrating sample, the pick-up coils are stationary. Voltage is generated in stationary pick-up coils by changes in the applied magnetic field.[39].



Fig 3.8 VSM

3.7.2 Different Parts of VSM

Following are the major parts of VSM.

- Water Cooled Electromagnet
- Sample Holder and Vibration Exciter
- Sensor Coils and Amplifier
- Lock-in Amplifier
- Computer Interface

3.7.2.1 Water Cooled Electromagnet

A water-cooled electromagnet with a power supply provides the steady magnetic field necessary to magnetize a sample.

3.7.2.2 Sample Holder and Vibration Exciter

A sample rod holds the sample between the pick-up coil pole components. The sample rod is connected to a vibration exciter, which vibrates the sample at a constant frequency. By rotating the sample rod, different directions of the specimen can be exposed to a steady magnetic field. A chassis controls the oscillation of the vibration exciter.

3.7.2.3 Sensor Coils and Amplifier

Alternating current is created in these sensor coils as the sample vibrates at a set frequency. The attached amplifier amplifies signals provided by sensing coils to check the magnetization of the sample.

3.7.2.4 Lock-in Amplifier

This enhances the signals by eliminating noise from the environment and capturing only the signals from the vibrating sample.

3.7.2.5 Computer Interface

The facilitates data collecting by controlling numerous components throughout the procedure.

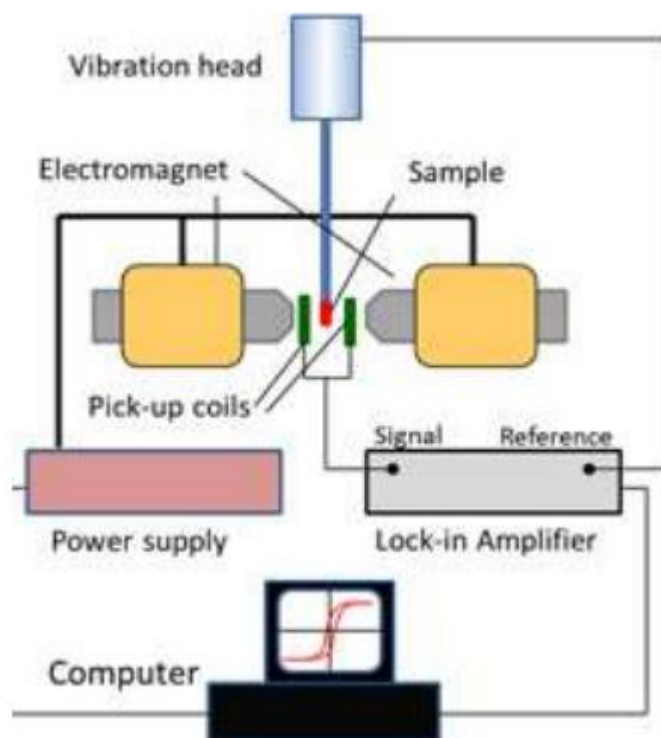


Fig 3.9 Diagram VSM

3.7.3 Precautions of VSM

1. To thoroughly saturate the samples, a magnetic field must be strong enough (or else inaccurate measurements will be taken)
2. The sample space's magnetic field must be uniform; otherwise, the inclusion of field gradients may create force that will again cause the vibration to change, giving erroneous data.

3.8 Dielectric Sample Preparation

Each sample (0.8g) was finely processed to form pellets 13mm in diameter using a hydraulic press equipment at 5 tons of pressure for 5 minutes. The produced pellets were then sintered in a furnace at 800 °C for 3 hours. Each pellet's thickness was measured with a Vernier caliper and used to calculate electrical parameters such as dielectric constant, dielectric loss, and permittivity.

3.8.1 DC Electrical Resistivity Measurement

DC resistivity was measured using the well-known two-probe method.

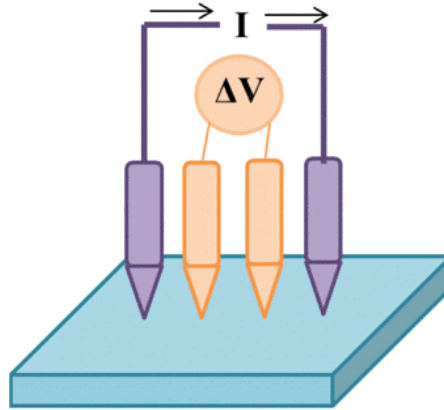


Fig 3.10 Illustration of two-probe method instrument setup

3.8.2 Dielectric Properties Measurement

The WAYNE KERR Precision Impedance Analyzer 6500B was used to calculate the dielectric characteristics of materials (in pellet form) while they were at room temperature. Ferrites rely heavily on their dielectric characteristics. Especially when it comes to the materials used in memory devices. Because of the small sample sizes in the nanoscale range, dielectric characteristics become extremely critical. These are the ferrites excellent dielectric materials. These have a variety of uses ranging from radio frequency to microwave frequency. This is necessary for studying the dielectric characteristics of ferrites at various frequency ranges. The processes used to prepare the ferrites have a significant impact on their dielectric characteristics. At room temperature, the dielectric constant is measured from 100 Hz to 5 MHz. The dielectric constant can be measured accurately. The dielectric constant can be calculated using the relationship given as

$$\varepsilon' = Cd / A \varepsilon_0$$

Where (A) is the area of the pellet, (d) is the thickness of the pellet, (C) is the capacitance, and (ε_0) is the free space permittivity.

3.9 Dielectric Loss Measurement

Dielectric loss (imaginary part of dielectric) corresponds to energy dissipation losses. It was calculated by the equation

$$\varepsilon'' = \varepsilon' \tan \delta$$

Dielectric losses in the radio frequency range are typically caused by dipole rotation. At lower frequencies, dielectric losses are mostly caused by dc resistivity. Dielectric losses are associated with electrons in the optical series of frequencies, and they are designated as optical absorption.

3.10 Tangent Loss Factor

The tangent loss factor that's the ratio of the dielectric loss to the dielectric constant. It is calculated by the following equation;

$$\tan \delta = \varepsilon'' / \varepsilon'$$

3.11 AC Conductivity Measurement

At normal temperature, AC conductivity was measured over a frequency range of 100 Hz to 5 MHz. It demonstrates the material's conductive properties as well as its hopping process. The following equation was used to compute it from the dielectric parameters:

$$\sigma = 2\pi f \tan\delta \varepsilon' \varepsilon$$

3.12 AC impedance Spectroscopy

At room temperature, the AC impedance properties of the samples were measured. Resistance (R) and reactance (X) were measured throughout a frequency range of 100 Hz to 5 MHz. The impedance is a complex number in which the relation between resistance (R) and reactance (X) displays the real and imaginary parts of the impedance in the circuit.

$$Z = R + jX$$

Chapter 4

Results and Discussion

4.1 XRD Analysis

At room temperature, the crystalline phase of all samples was recognised. by their XRD pattern obtained from their powder form. The XRD pattern was analyzed using the PANalytical X'Pert Highscore Pro software.

Powder diffraction machine 2d phaser by bruker uses CuK α (1.54060 Å) as a radiation source operated at 300 watts. Data was collected using the following parameters.

- Start position [2 Theta] = 20°
- End position [°2 Theta] = 80°
- Step size [°2 Theta] = 0.0500
- Scan step time [s] = 1.0000

The powder XRD patterns of Zn_{0.2}Ni_{0.3}Co_{0.5}Fe₂O₄ and MWCNTs nanocomposite. The single-phase spinel structure is confirmed by well-defined sharp diffraction peaks. All five samples have correctly separated peaks in the graph above. I calcined the pure ferrites samples at 800° C, and the results corroborated the spinel cubic structure. After the dispersion process to make nanocomposite of ferrites with multi walled carbon nanotubes the samples were again placed in oven at 200° C for 24 hours to dry them of dispersion medium. Prior to the XRD the samples were crushed using mortar and pestle. As reported by Contreras-Navarrete, J.J. et.al the MWCNTs begin to oxidized at the temperature of 270° C [40]. This is why samples were not calcinated again after the dispersion process to make ferrites with MWCNTs nanocomposites.

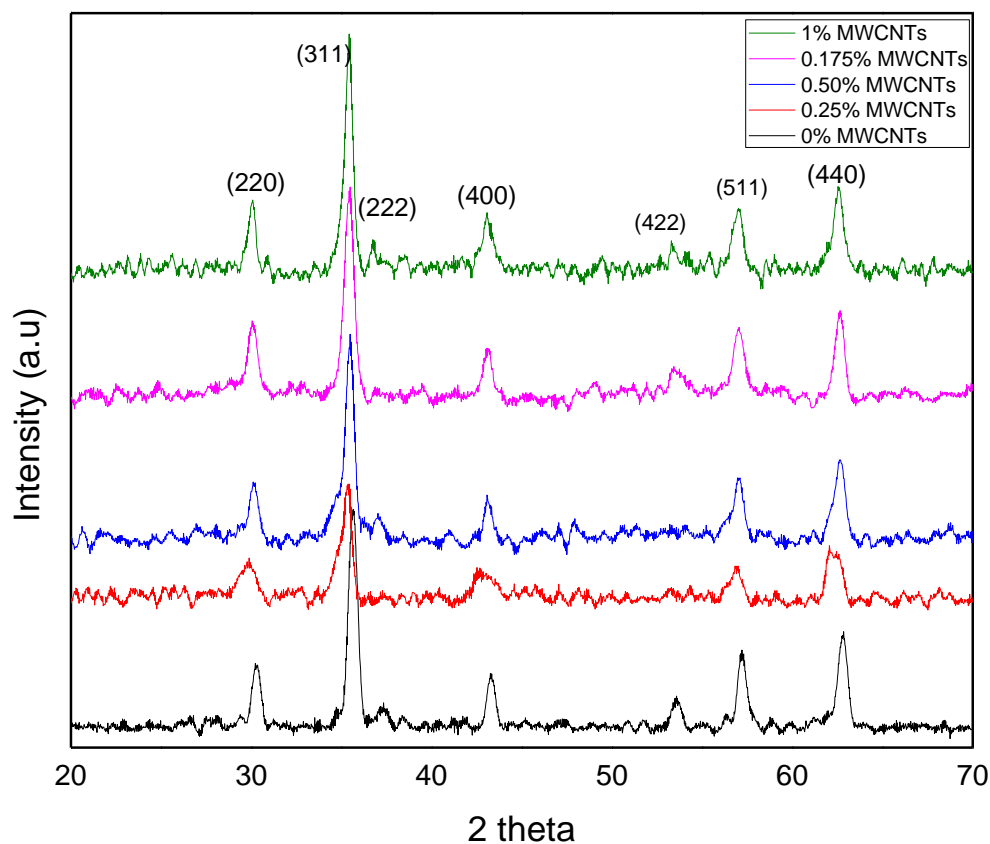


Fig 4.1 The X-Ray diffraction Pattern of $Zn_{0.2}Ni_{0.3}Co_{0.5}Fe_2O_4$ and $Zn_{0.2}Ni_{0.3}Co_{0.5}Fe_2O_4$ MWCNTs Nanocomposites

According to card number JCPDS-ICDD No. 022-1086, 10-0325, and 22-1012 all of the samples displayed well-resolved diffraction peaks at $2\theta = 30.2, 35.7, 37.4, 43.2, 53.5, 57.2, \text{ and } 62.8$ correspond to (220), (311), (222), (400), (422), (511), and (440) crystal planes. This proves synthesized $Zn_{0.2}Ni_{0.3}Co_{0.5}Fe_2O_4$ is crystalline in nature. It does not contain a second phase. The pattern may be seen to have a little increase in intensity between 25 and 28. This increase in intensity can be attributed to the limited detection of graphitic MWCNTs. According to studies, when MWCNTs are loaded to more than 15%, a distinct peak develops at $2\theta = 26.0^\circ$, which corresponds to the graphitic reflection of MWCNTs. The second point is the progressive increase in the peak's FWHM (311). This increase accounts for smaller and smaller crystallite size can be explained by the fact that the MWCNTs form networks at the grain boundaries as well as within the grains, cutting the grains from within and causing the grains to

shrink in size. The strength of the peak (311) also decreases with increasing MWCNT concentration, indicating a decrease in crystallinity due to the creation of more and more defects with rising MWCNT concentration. Using the Debye's Scherer equation, the average crystallite size for each XRD Pattern was calculated from the highest intense peak (311). The average crystallite size was discovered to be between 12.8 and 18.2 nm, indicating the production of tiny grain sizes. The decrease in crystallite size with increasing MWCNT concentrations corresponds to an increase in the FWHM of the associated peaks as the conductive MWCNTs network cuts through the grains, hence decreasing crystallite size.

4.2 Fourier Transform Infrared Spectroscopy

All MWCNT composite and pure samples had FTIR spectra that ranged in frequency from 400 cm to 4000 cm. Prior to FTIR measurement, the powder samples were combined with KBr, formed into pellets, and heated for one hour at 60 °C to dry them out. $Zn_{0.2}Ni_{0.3}Co_{0.5}Fe_2O_4$ /MWCNTs nanocomposites FTIR spectra were examined in the 400–4000 cm^{-1} frequency range, which is the range of frequencies commonly used to measure the compositions of the ferrites and MWCNTs samples [41-43]. The formation of different kinds of bound in crystals through ionic, covalent, or Van der Waals forces can be understood from the FTIR spectra.

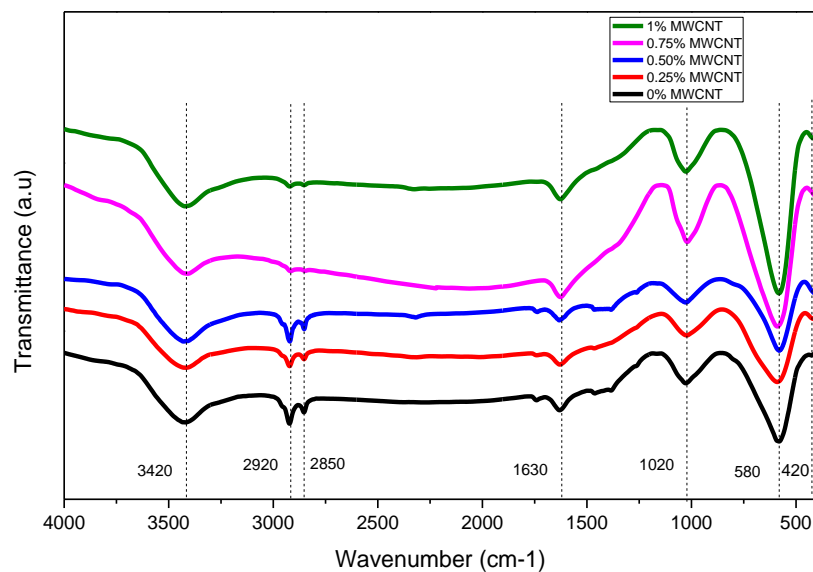


Fig 4.2 The FTIR Spectra of $Zn_{0.2}Ni_{0.3}Co_{0.5}Fe_2O_4$ and $Zn_{0.2}Ni_{0.3}Co_{0.5}Fe_2O_4$ /MWCNTs Nanocomposites

Tetrahedral (A) and Octahedral (B) sites are represented by two prominent absorption bands, ν_1 about 580 cm^{-1} and ν_2 around 420 cm^{-1} , respectively. The metal-oxygen stretching vibration mode at sites A and B is responsible for these ν_1 and ν_2 absorption bands [44]. These two sub-lattices bands' emergence in the FTIR spectrum supported the creation of single-phase spinel structure and was consistent with earlier findings [45]. The O-H stretch, which links to the -OH group bonded to the metal oxide surface, is represented by the wide frequency range between $3664\text{--}3100\text{ cm}^{-1}$ [46]. This shows that the water molecules were chemically adsorbed by the metal surface during the synthesis process. The C=C bond was responsible for the peak at 1630 cm^{-1} [47]. The peak around 1020 cm^{-1} is due to -OH out of plane bend [48]. The peaks around 2850 and 2920 cm^{-1} are due to the C-H bond stretching [49].

4.3 Scanning Electron Microscope

SEM is a very valuable technique for learning about microstructures, phase formation, grain/crystallite size, and sample composition. The samples were prepared in solution form for SEM investigation by dissolving the sample powder in toluene and sonicating it for 1 hour. Sonication is used to break apart particle clusters in order to obtain clear images. The possibilities of shattering clusters and obtaining clear images rise as the sonication time is increased. The results revealed that there are no clusters in the solution. Dispersion in polar solvent gives these nanocrystals enough time to arrange themselves to the lowest interfacial configuration. MWCNTs are entirely coated with nano-crystals, confirming the efficacy of our production method.

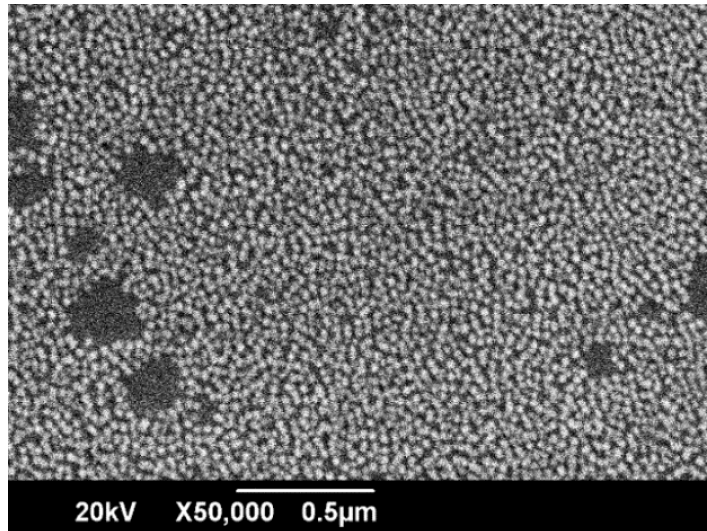


Fig 4.3 SEM image of $Zn_{0.2}Ni_{0.3}Co_{0.5}Fe_2O_4$ Nanoparticles

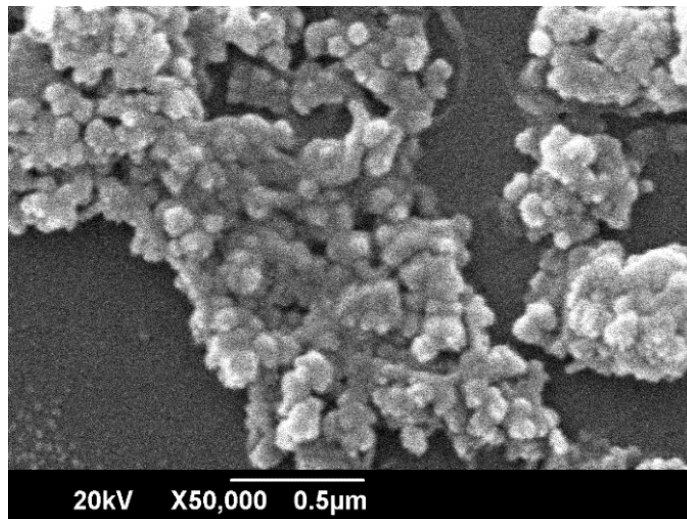


Fig 4.4 SEM image of $Zn_{0.2}Ni_{0.3}Co_{0.5}Fe_2O_4$ / wt% 0.25 MWCNTs Nanocomposite

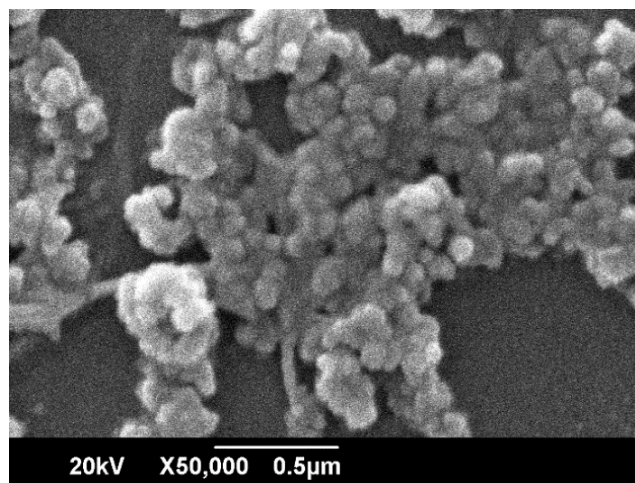


Fig 4.5 SEM image of $Zn_{0.2}Ni_{0.3}Co_{0.5}Fe_2O_4$ / wt% 0.50 MWCNTs Nanocomposite

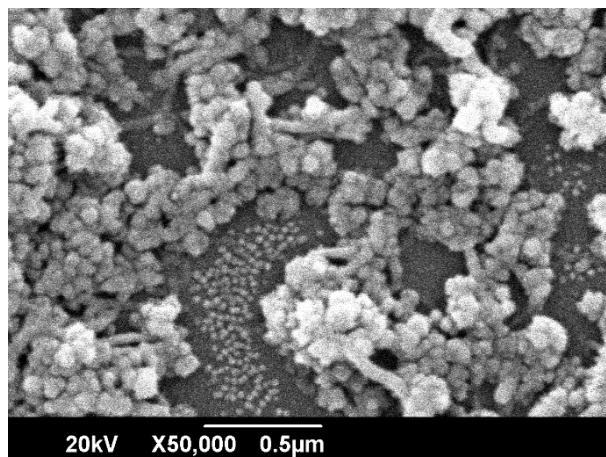


Fig 4.6 SEM image of $Zn_{0.2}Ni_{0.3}Co_{0.5}Fe_2O_4$ / wt% 0.75 MWCNTs Nanocomposite

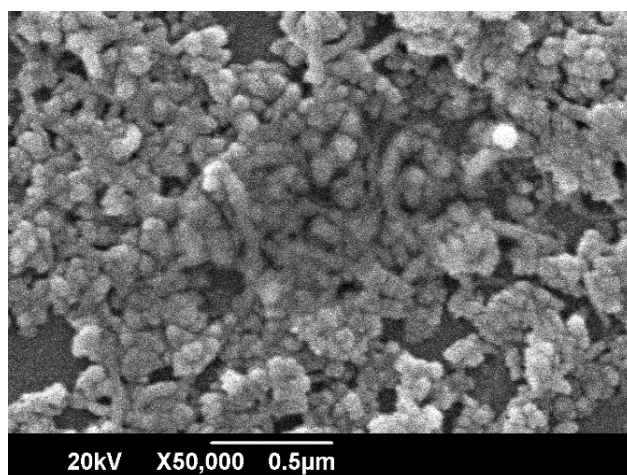


Fig 4.7 SEM image of $Zn_{0.2}Ni_{0.3}Co_{0.5}Fe_2O_4$ / wt% 1 MWCNTs Nanocomposite

The prepared samples particle shape and size were examined using SEM. The homogeneous dispersion of ferrites nanoparticles is depicted in Fig 4. Additionally, image (b) shows that the MWCNTs were covered with $Zn_{0.2}Ni_{0.3}Co_{0.5}Fe_2O_4$ nanoparticles, demonstrating the excellent efficacy of the dispersion process. The particle size varied between 14nm to 30nm, while average size being 20nm. All the sample contains different amount of weight percentage of MWCNT shows MWCNT. Particles can be seen to be agglomerate on the CNTs. Rest of the slide represent the sea of nanoparticles. This proves the composite is perfectly made. Average particle size of 18 nm remain the same for all the samples.

4.4 Energy Dispersive X-ray Spectrometry

EDX can be used to determine the atomic concentrations of various compositions. Energy dispersive x-rays were used to confirm the element compositions of prepared samples. Fig 4.9 to Fig 4.13 shows the EDX of Zn-Ni substituted Co ferrites and ferrites/MWCNTs nanocomposite. The very low intensity peaks in the samples can be due to the presence of impurities in the material. Figures confirmed the existence of Zinc, Nickel, Cobalt, Iron, Carbon and Oxygen. Tables confirmed the atomic percent and weight percent.

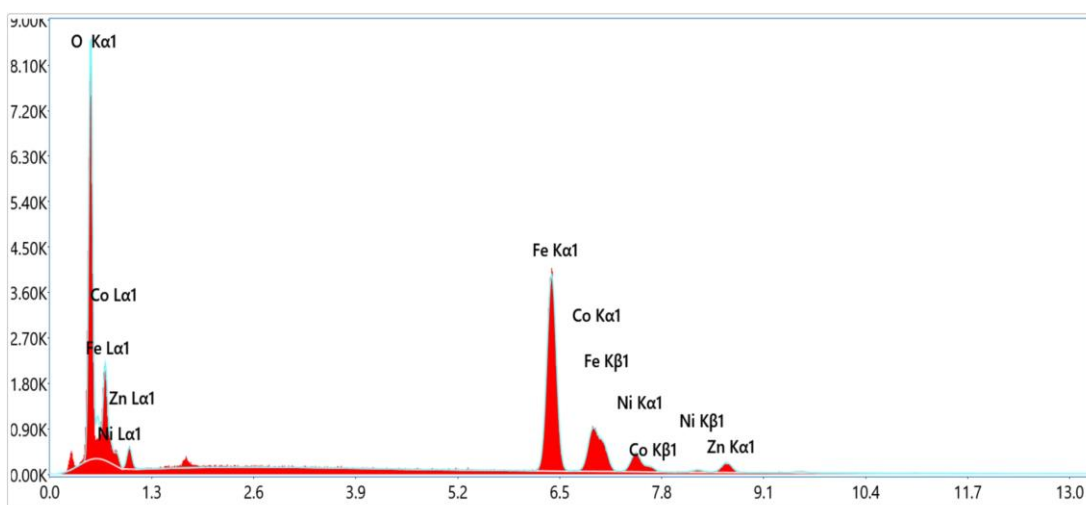


Fig 4.8 The EDX spectrum of Zn_{0.2}Ni_{0.3}Co_{0.5}Fe₂O₄

Table 1 Zn_{0.2}Ni_{0.3}Co_{0.5}Fe₂O₄ Atomic and Weight percentage

Element	Weight %	Atomic %
O	30.1	60.7
Fe	46.6	26.9
Co	11.8	6.4
Ni	6.2	3.4
Zn	5.2	2.6

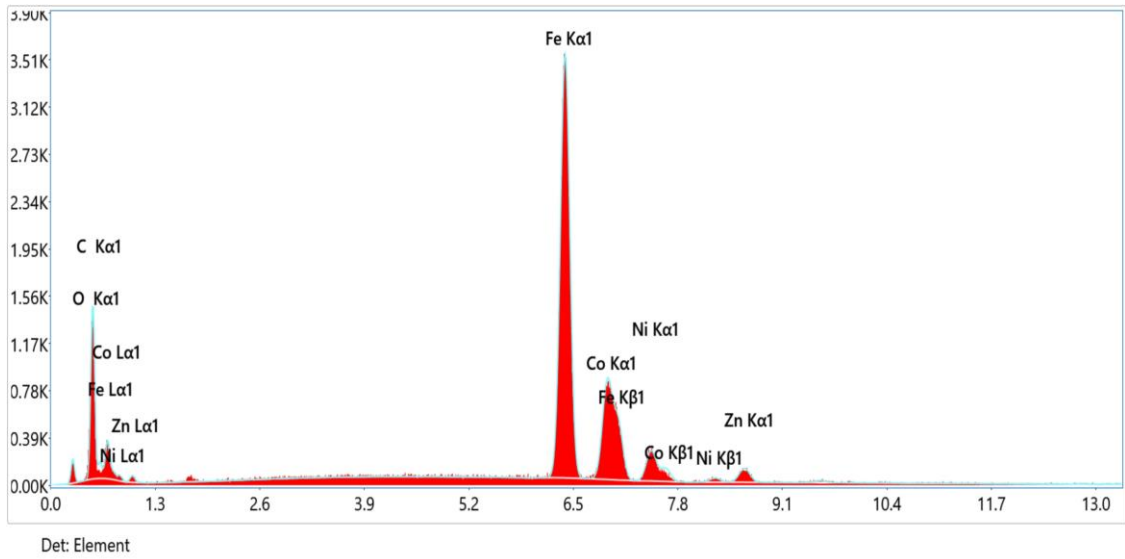


Fig 4.9 The EDX spectrum of $Zn_{0.2}Ni_{0.3}Co_{0.5}Fe_2O_4$ /0.25% wt MWCNTs

Table 2 $Zn_{0.2}Ni_{0.3}Co_{0.5}Fe_2O_4$ /0.25% wt MWCNTs Weight and Atomic percentage

Element	Weight %	Atomic %
C	5.1	16.9
O	9.2	22.9
Fe	58.7	42.1
Co	16.4	11.1
Ni	6.2	4.3
Zn	4.5	2.7

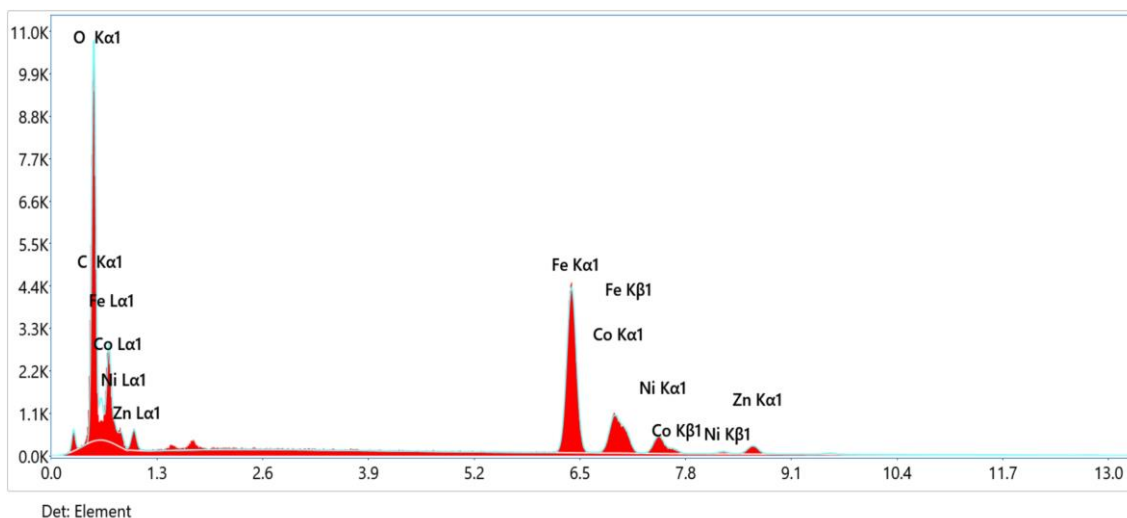


Fig 4.10 The EDX spectrum of $Zn_{0.2}Ni_{0.3}Co_{0.5}Fe_2O_4/0.5\%$ wt MWCNTs

Table 3 $Zn_{0.2}Ni_{0.3}Co_{0.5}Fe_2O_4/0.5\%$ wt MWCNTs Weight and Atomic percentage

Element	Weight %	Atomic %
C	6.6	14.9
O	33.4	56.6
Fe	39.5	19.2
Co	10.2	4.7
Ni	5.8	2.7
Zn	4.4	1.8

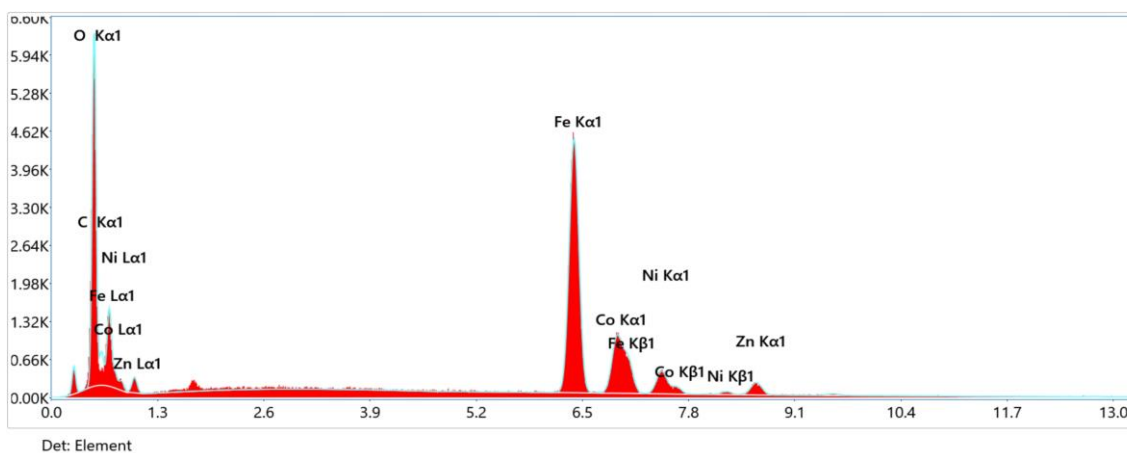


Fig 4.11 The EDX spectrum of $Zn_{0.2}Ni_{0.3}Co_{0.5}Fe_2O_4/0.75\%$ wt MWCNTs

Table 4 $Zn_{0.2}Ni_{0.3}Co_{0.5}Fe_2O_4/0.75\%$ wt MWCNTs Weight and Atomic percentage

Element	Weight %	Atomic %
C	7.0	17.7
O	23.8	45.3
Fe	46.1	25.2
Co	12.0	6.2
Ni	5.9	3.1
Zn	5.1	2.4

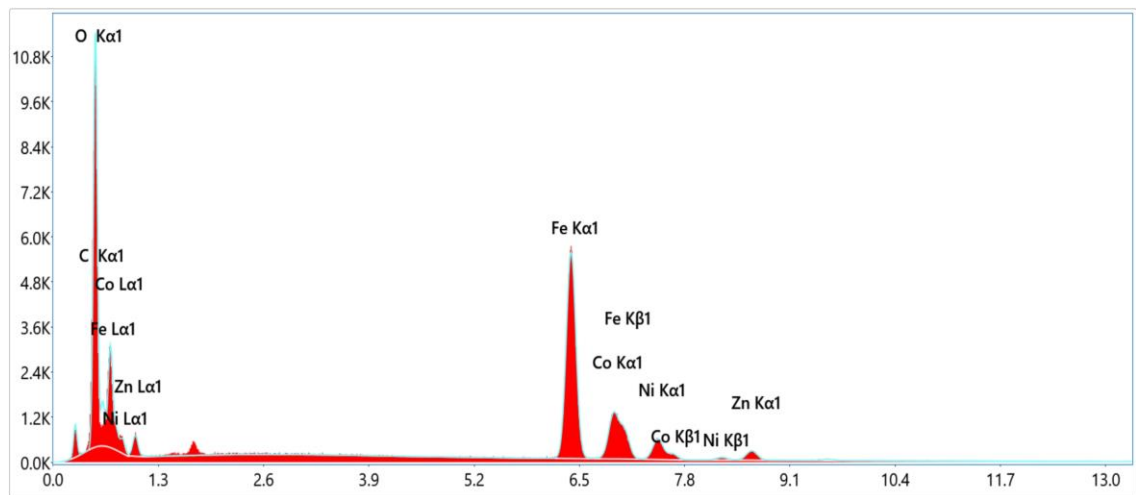


Fig 4.12 The EDX spectrum of $Zn_{0.2}Ni_{0.3}Co_{0.5}Fe_2O_4/ 1\%$ wt MWCNTs

Table 5 $Zn_{0.2}Ni_{0.3}Co_{0.5}Fe_2O_4/1\%$ wt MWCNTs Weight and Atomic

Element	Weight %	Atomic %
C	8.4	19.2
O	30.3	51.6
Fe	41.0	20.0
Co	10.4	4.8
Ni	5.7	2.7
Zn	4.2	1.7

4.5 Dielectric Properties

Dielectric properties of $\text{Zn}_{0.2}\text{Ni}_{0.3}\text{Co}_{0.5}\text{Fe}_2\text{O}_4$ /MWCNTs wt.% = (0-1) % Solid powder pallets pressed at 5ton for 5 minutes with a 13mm dye were made to analyze their dielectric properties. Pallets were placed in furnace for 3 hours at temperature of 270°C to sintered [50]. Temperature was carefully chosen to avoid oxidation of MWCNTs present in the composite. The variation of dielectric constant ϵ' against alternating frequency 100 Hz to 5 MHz for the synthesized compositions of $\text{Zn}_{0.2}\text{Ni}_{0.3}\text{Co}_{0.5}\text{Fe}_2\text{O}_4$ /MWCNTs composites were taken at room temperature is shown in Fig. When a material is exposed to an externally applied ac-field, the real part of the dielectric constant, which is provided by the following relation, gives the stored energy.

$$\epsilon' = C d/A \epsilon_0$$

where C, d, A and ϵ_0 are the capacitance, thickness of the sample's pellet, surface area of the pellets ($A=\pi r^2$) and ϵ_0 is the permittivity of free space (8.854×10^{-12}) respectively [51]. It can be seen in Fig 32 that high ϵ' value observed at low frequency range, while it decreases with increasing frequency. It can also be observed from the graph that with increase in the quantity of the MWCNTs the value of ϵ' also increased. The value of ϵ' reduced as frequency values increased because dipoles were unable to align themselves with the applied ac-field, which resulted in diminished space-charge polarizations [52]. The dielectric response of $\text{Zn}_{0.2}\text{Ni}_{0.3}\text{Co}_{0.5}\text{Fe}_2\text{O}_4$ /MWCNTs nanocomposites was studied using Koop's model and Maxwell's Wagner theory, which assert that these nanocomposites consist of microscopic granules, which are typically conductors, splitted across grain boundaries, which are typically insulators. At lower frequencies, grains are more active, whereas at higher frequencies, they are more resistant grain-boundaries lack this phenomenon, leading electrons to accumulate across them and creating polarization. Therefore, the migration of the electron occurs from grain to grain boundary at lower frequencies, leading to greater values of ϵ' at lower frequencies. Hence ϵ' displays minimal values. Additionally, at higher frequencies, this pattern is considerably different because it is challenging for electrons to flow from grains toward grain borders that have high grain resistance between Fe^{+2} and Fe^{+3} . As a result, sample exhibits low values in the high frequency region since the electrons can't hop [53].

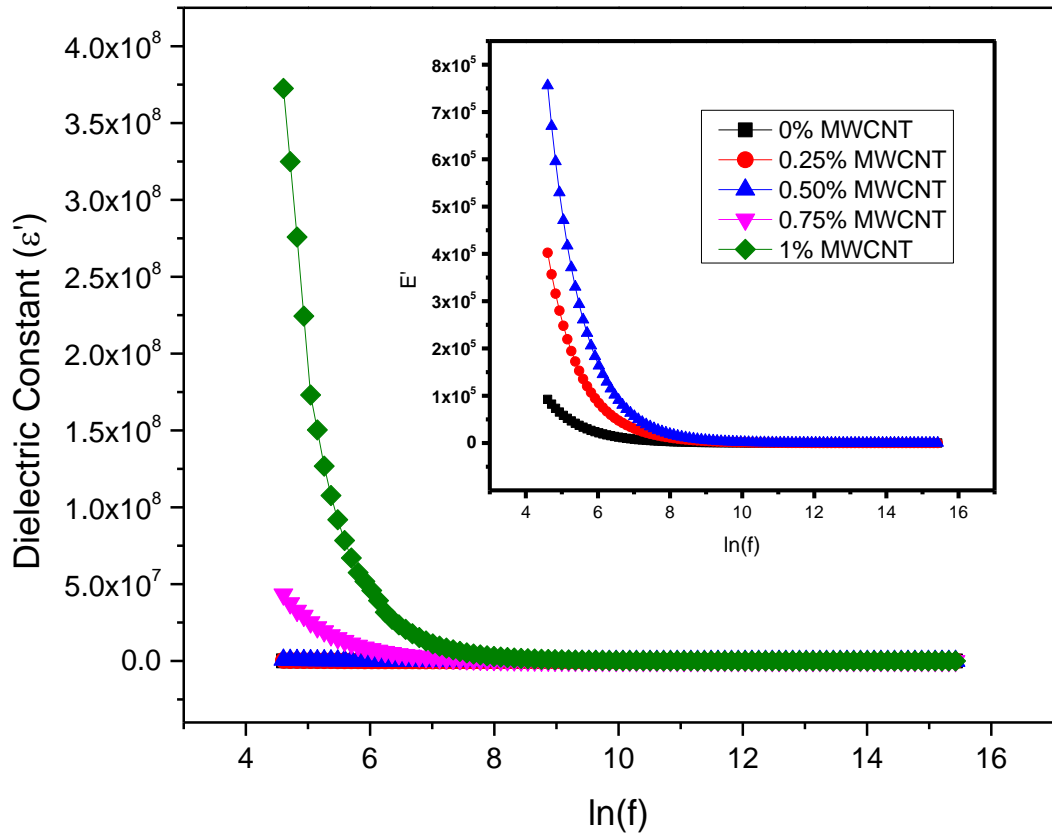


Fig 4.13 Variation of Dielectric Constant with Frequency of $Zn_{0.2}Ni_{0.3}Co_{0.5}Fe_2O_4$ and $Zn_{0.2}Ni_{0.3}Co_{0.5}Fe_2O_4$ / MWCNTs Nanocomposites

It can also be seen in Fig 32 that by increasing the weight % of MWCNTs in the material the ϵ' kept increasing. This is due to the conductive nature of MWCNTs. MWCNTs form carbon network in the material [54]. This enhanced the conductive nature ZCNF/MWCNTs nanocomposites. All the energy of incoming wave cannot be stored as dielectric energy, some of it can be wasted as heat due to skin effect. This form of energy lost can be observed by calculating the imaginary part of dielectric constant ϵ'' . The imaginary part of dielectric constant ϵ'' can be calculated using the formula.

$$\epsilon'' = \epsilon' \tan \delta$$

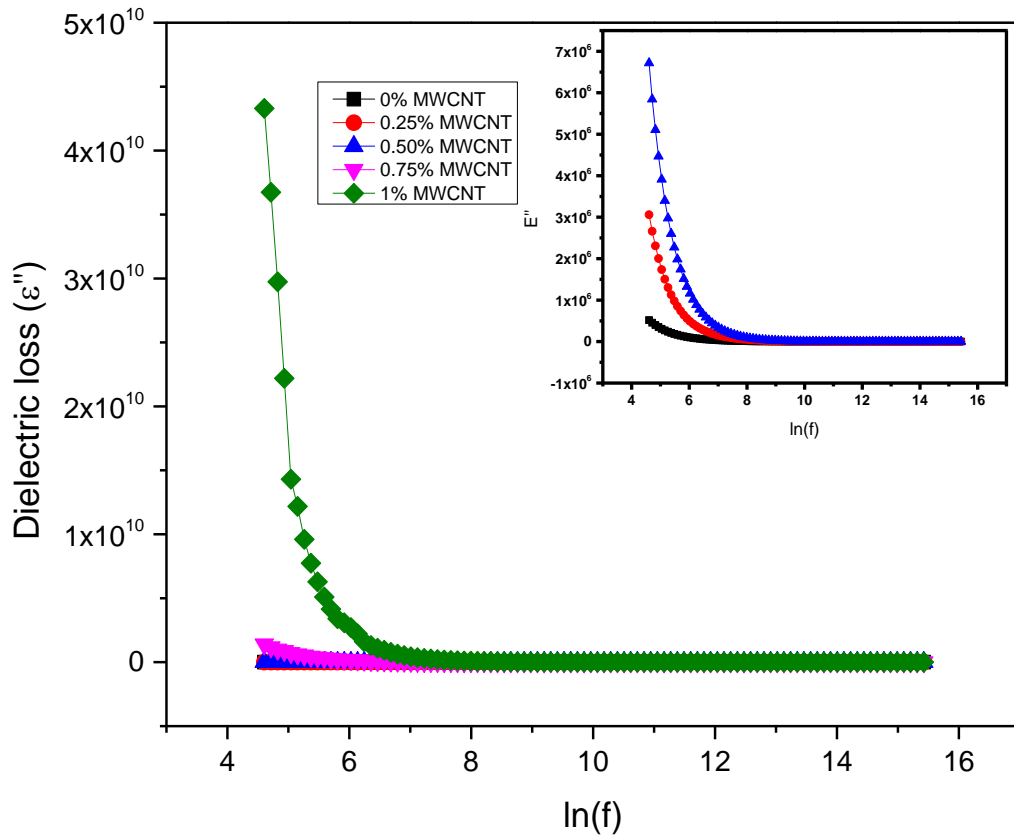


Fig 4.14 Imaginary part Dielectric Constant with Frequency of $Zn_{0.2}Ni_{0.3}Co_{0.5}Fe_2O_4$ and $Zn_{0.2}Ni_{0.3}Co_{0.5}Fe_2O_4$ / MWCNTs Nanocomposites

Fig 33 present the ϵ'' of the material as a function of frequency. We can observe as the composition of MWCNTs increases in $Zn_{0.2}Ni_{0.3}Co_{0.5}Fe_2O_4$ the ϵ'' increases as well. The ϵ'' exhibits maximum values in the lower frequency range, a declining trend in the higher frequency range, and constant values beyond those frequencies. According to the Fig 33, the value of ϵ'' rises as the amount of MWCNTs in these nanocomposites increases, which may be clarified by the growth in the number of voids between $Zn_{0.2}Ni_{0.3}Co_{0.5}Fe_2O_4$ nanoparticles and MWCNTs. This could also be attributed to the development of π -bonds and the increased surface area of MWCNTs.

4.6 Tangent Loss Factor

Dielectric loss tangent of a dielectric material is a factor that affects how much electromagnetic energy or current is lost in the material [55]. Particularly in capacitor materials or bridge circuits, the dielectric loss or tangent loss is a crucial measurement

to determine the suitability of any material for electrical applications. The dielectric loss of $Zn_{0.2}Ni_{0.3}Co_{0.5}Fe_2O_4$ /MWCNTs wt.% = (0-1) % were examined at frequency range 100Hz to 5Mhz. It was observed that the value of $Tan \delta$ was maximum at lower frequency and decreases with the increasing frequency. The Koop's and Maxwell-Wagner Model is also confirmed by the fact that the decrease in $\tan \delta$ with frequency was caused by a decrease in space-charge polarization, which becomes minimal and constant at a given high frequency [56].

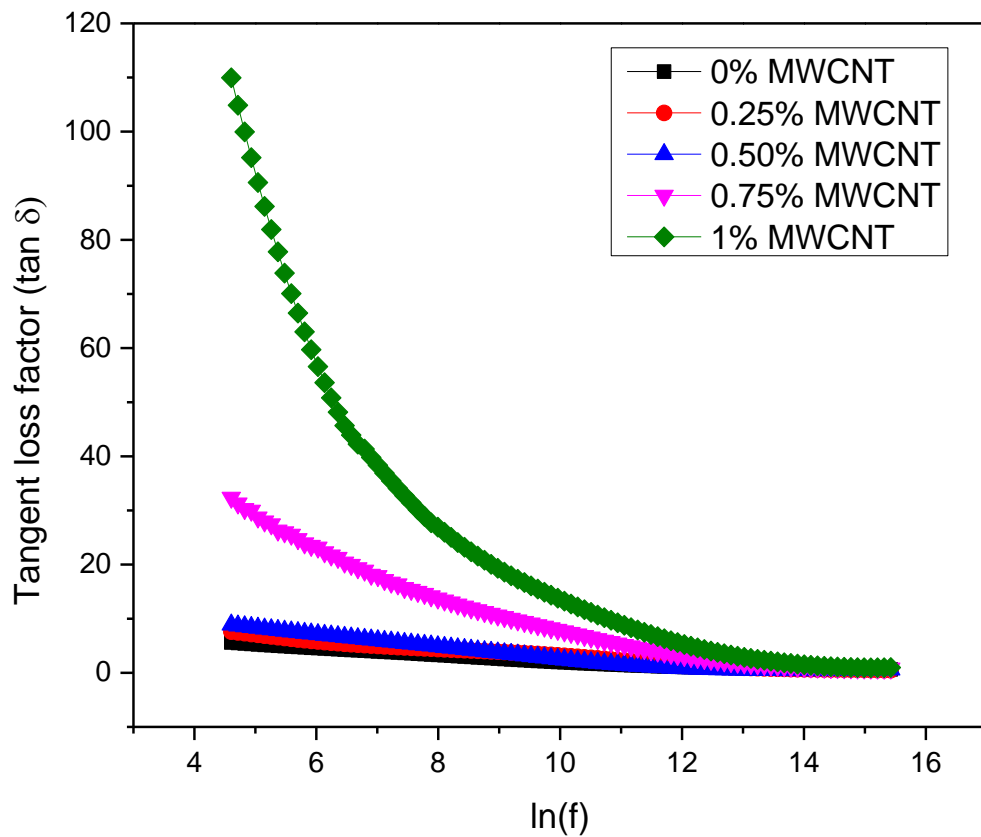


Fig 4.15 Dielectric loss tangent as a function of Frequency of $Zn_{0.2}Ni_{0.3}Co_{0.5}Fe_2O_4$ and $Zn_{0.2}Ni_{0.3}Co_{0.5}Fe_2O_4$ / MWCNTs Nanocomposites

4.7 Impedance

Impedance analysis is a potent technique that may be used to directly link microstructure with nanomaterials' thermal properties. The thermal properties of nanomaterials are affected by their size, shape, surfacing atoms, and microstructure [57]. Impedance between 100 Hz and 5 MHz was observed. Impedance spectroscopy,

which considers the complex impedance of nanomaterials, is used to modify the electrical characterization.

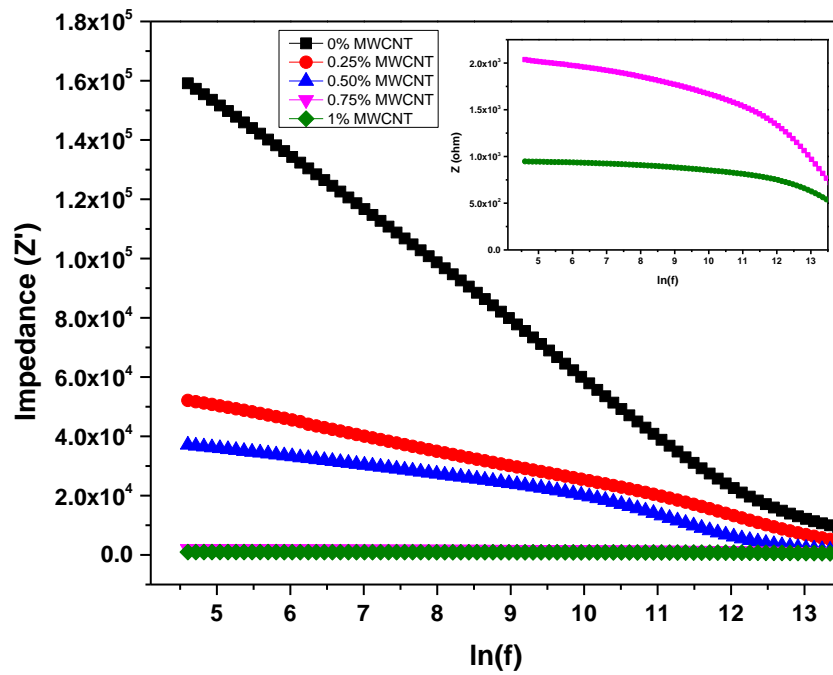


Fig 4.16 Variation of Z' Versus Frequency for $Zn_{0.2}Ni_{0.3}Co_{0.5}Fe_2O_4$ and $Zn_{0.2}Ni_{0.3}Co_{0.5}Fe_2O_4$ / MWCNTs Nanocomposites

With the increase in the composition of MWCNTs, the impedance of sample is seen dropping. This is because of increase in conductivity due to the conductive nature of MWCNTs. As seen in DC conductivity two probe experiment, the conductivity of the samples increases with the increase in the percentage weight of MWCNTs.

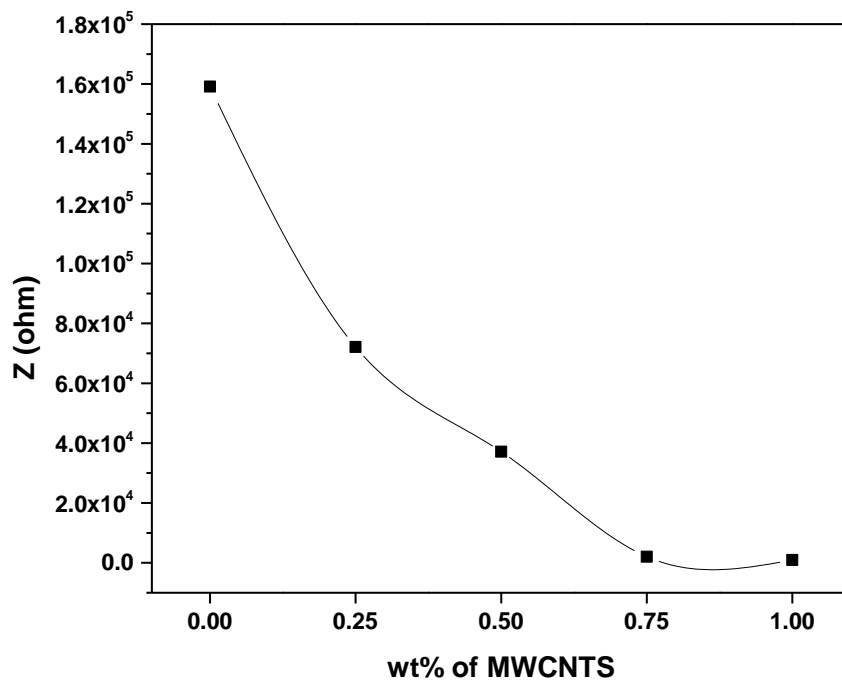


Fig 4.17 Impedance at 100 Hz

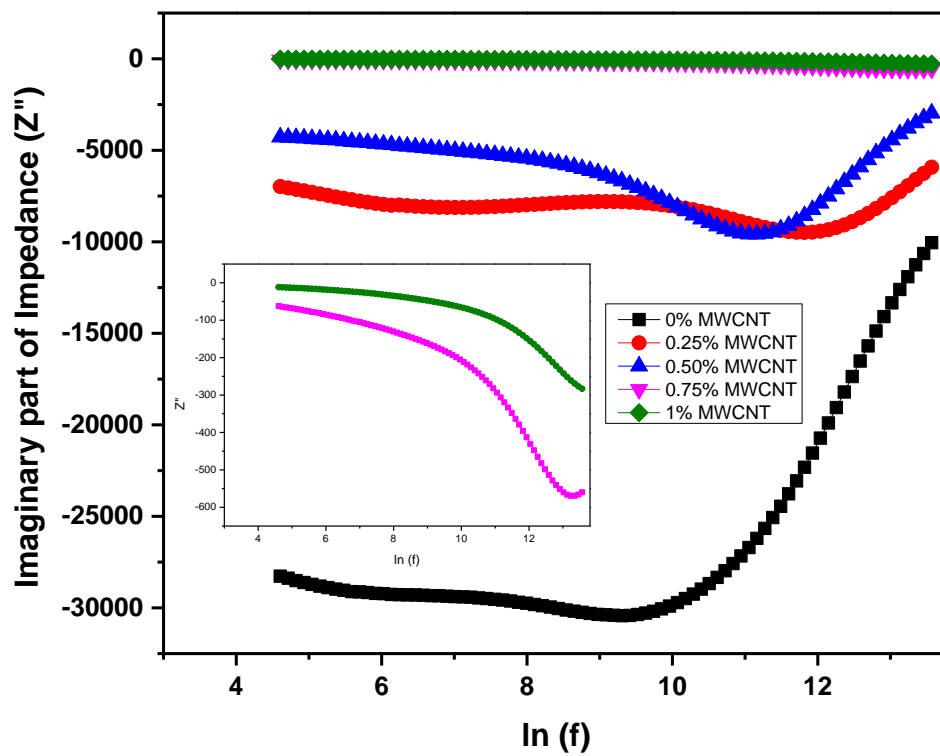


Fig 4.18 Variation of Z'' Versus frequency for $Zn_{0.2}Ni_{0.3}Co_{0.5}Fe_2O_4$ and $Zn_{0.2}Ni_{0.3}Co_{0.5}Fe_2O_4$ / MWCNTs Nanocomposites

Fig 4.19 depicts the complex impedance of $Zn_{0.2}Ni_{0.3}Co_{0.5}Fe_2O_4/MWCNTs$ nanocomposites as it varies with frequency. It is evident that the magnitude of the real and imaginary parts of the impedance, which are frequency dependent, declined with frequency and became constant at higher frequencies. With increased frequency, the impedance falls, indicating that the conductivity of the $Zn_{0.2}Ni_{0.3}Co_{0.5}Fe_2O_4/MWCNTs$ samples has increased. Fig 4.18 displays the complex impedance graph's change with frequency at 100 Hz for the five $Zn_{0.2}Ni_{0.3}Co_{0.5}Fe_2O_4/MWCNTs$ samples.

4.8 AC Conductivity

The synthesized nanocomposite's activity in AC conductivity with increasing frequency has been presented in the Fig 4.20. As we can see the overall ac conductivity is increasing with increasing the composition of MWCNTs. The ac conductivity of samples decreases with the increasing frequency and then again rise at high frequency [31].

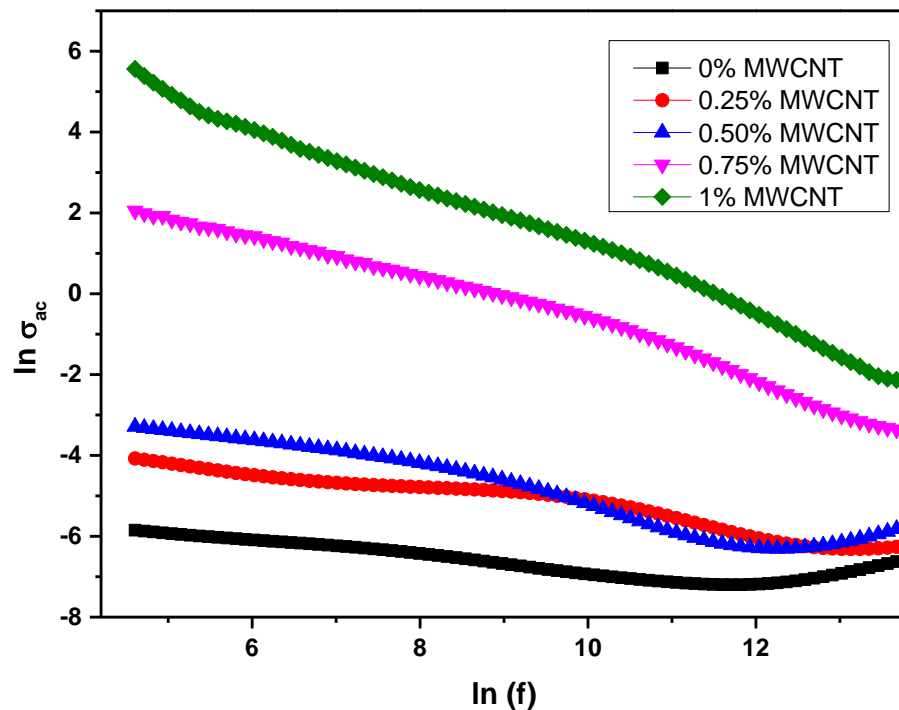


Fig 4.19 AC Conductivity Change as a Function of Frequency for $Zn_{0.2}Ni_{0.3}Co_{0.5}Fe_2O_4$ and $Zn_{0.2}Ni_{0.3}Co_{0.5}Fe_2O_4/MWCNTs$ Nanocomposites

The polarons are explanation for this pattern. Polarons are the correct term for electrons and holes in any conducting material. A polaron's radius can be "big" or "small," depending on how it relates to the lattice constant. Aside from size, the most significant distinction between large and small polarons is in their electrical transport: Large polarons typically undergo band-like transport, whereas small polarons typically experience hopping transport. for large polarons, AC-conductivity declines with rising frequency, whereas for small polarons, AC-conductivity increases with increasing frequency [32]. The dominance of hopping conduction over band conduction can be used to explain why it can be seen that AC-conductivity decreases with frequency and then increases in the high frequency zone

4.9 DC Conductivity

The DC conductivity of $Zn_{0.2}Ni_{0.3}Co_{0.5}Fe_2O_4$ /MWCNTs was measured using two probe method at room temperature. It can be observed that with increasing the composition of MWCNTs the conductivity of nanocomposites increases exponentially. Which can be explained by MWCNTs characteristics of forming network [58].

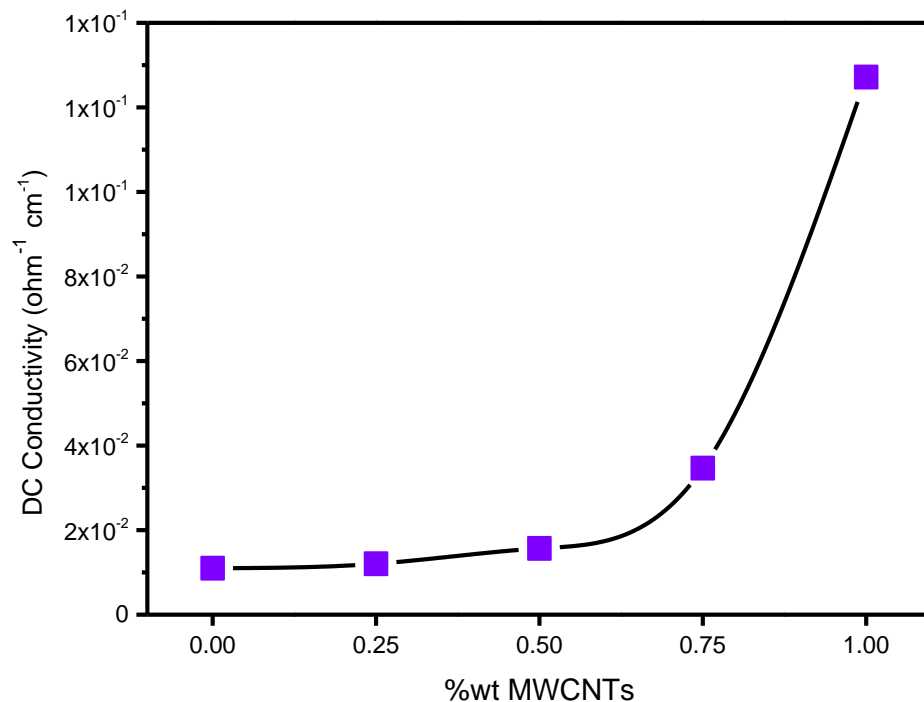


Fig 4.20 DC Conductivity Variation with Varying wt. % MWCNTs in Ferrites

A unit cell of graphene (a single brick that makes up the wall) is made up of four carbon atoms covalently connected to each other through sp^2 molecular orbitals - with the fourth valence electron, in the p_z orbital, hybridizing with the other p_z orbitals to form a delocalized π -band. As a result, every pair of carbon atom in the unit cell contains an even number of electrons, but the fourth electron is free to move, making the unit cell, and hence the entire wall of atoms, semi-conducting and metallic.

4.10 Vibrating Sample Magnetometer

Compared to the ZCNF ferrite made via co-precipitation synthesis, the ZCNF/MWCNTs nanocomposite saturation magnetization and coercivity are lower. It is evident that as the amount of carbon nanotubes increases, the saturation magnetization and coercivity fall.

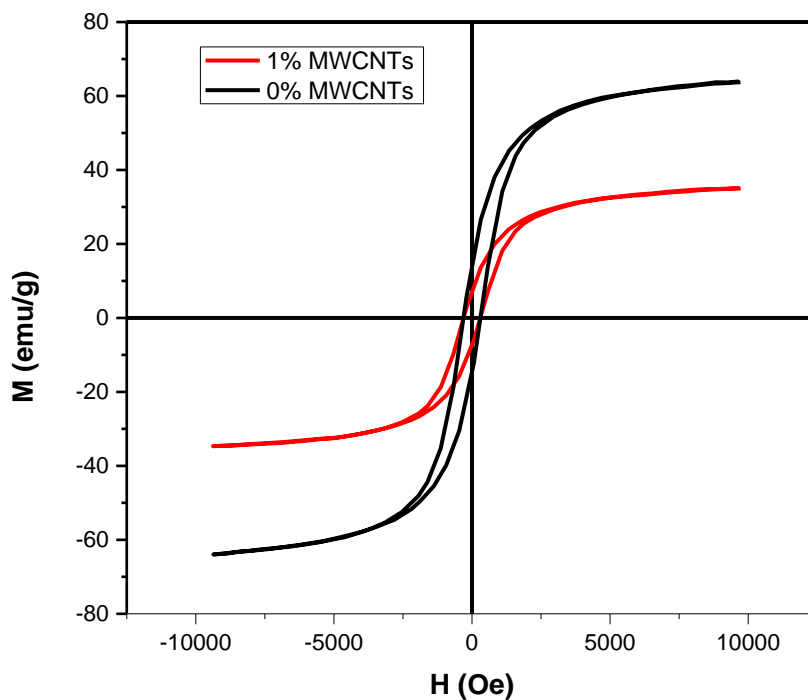


Fig 4.21 Magnetic Hysteresis Loop of $Zn_{0.2}Ni_{0.3}Co_{0.5}Fe_2O_4$ and $Zn_{0.2}Ni_{0.3}Co_{0.5}Fe_2O_4$ /MWCNTs Nanocomposites

Because the attachment of ferrite nanoparticles to MWCNTs is a completely random process, such subsequent drop in saturation magnetization could be connected to the quantity of magnetic particles and, as a result, the number of aligned spins per unit

volume. The nanocomposites are made up of MWCNTs and ferrite nanoparticles that have a completely random distribution. In fact, increasing the ferrite nanoparticles in the nanocomposite samples increases magnetism. As the replacement content grew from $x = 0$ to $x = 1$, the magnetism value fell due to a decrease in the ferrite nanoparticles.

Table 6 Table of magnetic properties of $Zn_{0.2}Ni_{0.3}Co_{0.5}Fe_2O_4$ and $Zn_{0.2}Ni_{0.3}Co_{0.5}Fe_2O_4$ / MWCNTs

Sample	Ms (emu/g)	Mr (emu/g)	Hc (Oe)
$Zn_{0.2}Ni_{0.3}Co_{0.5}Fe_2O_4$	63.7	13.63	310.07
$Zn_{0.2}Ni_{0.3}Co_{0.5}Fe_2O_4$ / 1% wt. MWCNTs	35.1	6.73	304.43

The existence of defects and strain in the nanocomposite structure acts as a barrier to magnetic domain migration, resulting in a decrease in saturation magnetization. Purified MWCNTs are well known to have paramagnetic properties, with very weak magnetization toward an applied magnetic field; magnetization of roughly 0.03 emu/g can be achieved for an applied field of 0.5 kOe. As a result, the addition of MWCNTs to the nanocomposite structure has a negative influence on magnetic properties such as saturation magnetization.

Conclusion

Using chemical co-precipitation method, the Zn-Ni substituted Co ferrites nanoparticles were synthesized. SEM images proved the synthesis of nanoparticles. The average particle size from SEM was 18 nm. XRD was done for the confirmation of single-phase synthesis of Zinc and nickel substituted cobalt ferrites. The average crystallite size for the zinc and nickel substituted cobalt ferrites measure by Debye-Scherrer equation was $15 \text{ nm} \pm 3 \text{ nm}$. The average crystallite size for each sample was in complete agreement with the results obtained from high resolution scanning electron microscope within experimental error. FTIR Spectra which showed band ranges of $570\text{-}590 \text{ cm}^{-1}$ for tetrahedral and $400\text{-}420 \text{ cm}^{-1}$ for octahedral lattice sites, further validated the structural creation of ferrites. With the help of ultrasonication, nanoparticles of ferrites were imbedded on the surface of MWCNTs. Toluene was used as a dispersion liquid for nanocomposite synthesis. The high surface area of MWCNTs, which created a conducting framework with the ferrites, greatly improved the dielectric characteristics. The dielectric loss factor also increased, indicating that modest MWCNT addition values would be excellent for high dielectric values with a low loss factor. This enhancement by the introduction of MWCNTs can be used in capacitors and electromagnetic interference shielding materials. The dielectric properties of Zinc and nickel substituted cobalt ferrites and their nanocomposite with multi walled carbon nanotubes were studied. The dielectric constant of pure Zn-Ni substituted Co ferrites is 1×10^5 whereas it has increased with the addition of MWCNTs. At wt. 1% MWCNTs, the dielectric constant is increased to 3.7×10^8 at frequency of 100 Hz. The A.C conductivity is maximum at lower frequency which represents the dominance of band conductivity over hopping conductivity. VSM analyses the emu/g of nanoparticles which turns out to be 63.7 emu/g for $\text{Zn}_{0.2}\text{Ni}_{0.3}\text{Co}_{0.5}\text{Fe}_2\text{O}_4$ nanoparticles and 35.1 emu/g for $\text{Zn}_{0.2}\text{Ni}_{0.3}\text{Co}_{0.5}\text{Fe}_2\text{O}_4/1\% \text{ wt. MWCNTs}$.

References

- [1] Ciambelli, P., G. La Guardia, and L. Vitale, Nanotechnology for green materials and processes, in *Studies in Surface Science and Catalysis*. (2020), Elsevier. p. 97-116.
- [2] Ghattas, N.I. and J.S. Carver, Secondary Ghattas, N.I. and J.S. Carver, *Research in Science & Technological Education*, (2012) 271-284.
- [3] Nasrollahzadeh, M., et al., Secondary Nasrollahzadeh, M., et al., *Interface science and technology*, (2019) 113-143.
- [4] Schaming, D. and H. Remita, Secondary Schaming, D. and H. Remita, *Foundations of Chemistry*, (2015) 187-205.
- [5] Sriram, P. and A. Suttee, *Nanotechnology advances, benefits, and applications in daily life*, in *Nanotechnology*. (2020), CRC Press. p. 23-44.
- [6] Subramanian, V. and T. Lee, Secondary Subramanian, V. and T. Lee, *Nanotechnology*, (2012) 340201.
- [7] Ferreira, M.A.M., J.A. Filipe, and J. Chavaglia. *Nanotechnology and processes the nanophotovoltaic panels*. in *Advanced Materials Research*. 2014. Trans Tech Publ.
- [8] Hussein, A.K., Secondary Hussein, A.K., *Renewable and Sustainable Energy Reviews*, (2016) 767-792.
- [9] Abdin, Z., et al., Secondary Abdin, Z., et al., *Renewable and sustainable energy reviews*, (2013) 837-852.
- [10] Wong, Y., et al., Secondary Wong, Y., et al., *AUTEX research Journal*, (2006) 1-8.
- [11] Salamati, M., et al., Secondary Salamati, M., et al., *Construction and Building Materials*, (2019) 477-482.

- [12] Taghiyari, H.R., et al., Nanotechnology for wood quality improvement and protection, in Nanomaterials for agriculture and forestry applications. (2020), Elsevier. p. 469-489.
- [13] Joshi, R.K. and J.J. Schneider, Secondary Joshi, R.K. and J.J. Schneider, Chemical Society Reviews, (2012) 5285-5312.
- [14] Lv, C., et al., Secondary Lv, C., et al., Chemical Society Reviews, (2021) 3957-3989.
- [15] Cao, X., et al., Secondary Cao, X., et al., Advanced Functional Materials, (2020) 2003618.
- [16] Wu, L., et al., Secondary Wu, L., et al., Journal of magnetism and magnetic materials, (2005) 233-239.
- [17] Che, M. and C.O. Bennett, The influence of particle size on the catalytic properties of supported metals, in Advances in Catalysis. (1989), Elsevier. p. 55-172.
- [18] Fu, S.-Y., et al., Secondary Fu, S.-Y., et al., Composites Part B: Engineering, (2008) 933-961.
- [19] Valenzuela, R., Secondary Valenzuela, R., Physics Research International, (2012).
- [20] Sugimoto, M., Secondary Sugimoto, M., Journal of the American Ceramic Society, (1999) 269-280.
- [21] Shaikh, S.F., et al., Types, synthesis methods and applications of ferrites, in Spinel Ferrite Nanostructures for Energy Storage Devices. (2020), Elsevier. p. 51-82.
- [22] Mohapatra, J., M. Xing, and J.P. Liu, Secondary Mohapatra, J., M. Xing, and J.P. Liu, Materials, (2019) 3208.
- [23] Amiri, M., M. Salavati-Niasari, and A. Akbari, Secondary Amiri, M., M. Salavati-Niasari, and A. Akbari, Advances in colloid and interface science, (2019) 29-44.

- [24] Kharat, P.B., et al. Effect of magnetic field on thermal conductivity of the cobalt ferrite magnetic nanofluids. in *Journal of Physics: Conference Series*. 2020. IOP Publishing.
- [25] Henderson, C., J. Charnock, and D. Plant, Secondary Henderson, C., J. Charnock, and D. Plant, *Journal of Physics: Condensed Matter*, (2007) 076214.
- [26] Shailaja, K., et al., Secondary Shailaja, K., et al., *Indian J Res Pharm Biotechnol*, (2013) 2321-5674.
- [27] Yang, D., et al., Secondary Yang, D., et al., *Physics Letters A*, (2004) 207-213.
- [28] Singh, C., S. Bansal, and S. Singhal, Secondary Singh, C., S. Bansal, and S. Singhal, *Physica B: Condensed Matter*, (2014) 70-76.
- [29] Amiri, S. and H. Shokrollahi, Secondary Amiri, S. and H. Shokrollahi, *Materials Science and Engineering: C*, (2013) 1-8.
- [30] Tourinho, F., et al., Secondary Tourinho, F., et al., *Trends in colloid and Interface science III*, (1989) 128-134.
- [31] Vatamanu, J., et al., Secondary Vatamanu, J., et al., *Journal of Materials Chemistry A*, (2017) 21049-21076.
- [32] Petcharoen, K. and A. Sirivat, Secondary Petcharoen, K. and A. Sirivat, *Materials Science and Engineering: B*, (2012) 421-427.
- [33] Millot, N., et al., Secondary Millot, N., et al., *Journal of the European Ceramic Society*, (2007) 921-926.
- [34] Mohamed, M.A., et al., Fourier transform infrared (FTIR) spectroscopy, in *Membrane characterization*. (2017), Elsevier. p. 3-29.
- [35] Zhou, W., et al., Fundamentals of scanning electron microscopy (SEM), in *Scanning microscopy for nanotechnology*. (2006), Springer. p. 1-40.
- [36] Vernon-Parry, K., Secondary Vernon-Parry, K., *III-Vs Review*, (2000) 40-44.

- [37] Rochow, T.G. and P.A. Tucker, Scanning Electron Microscopy and Compositional Analysis, in Introduction to Microscopy by Means of Light, Electrons, X Rays, or Acoustics. (1994), Springer. p. 297-327.
- [38] Heu, R., et al., Secondary Heu, R., et al., Microscopy Today, (2019) 32-36.
- [39] Adeyeye, A.O. and G. Shimon, Chapter 1 - Growth and Characterization of Magnetic Thin Film and Nanostructures, in Handbook of Surface Science, R.E. Camley, Z. Celinski, and R.L. Stamps, Editors. (2015), North-Holland. p. 1-41.
- [40] Contreras-Navarrete, J.J., et al., Secondary Contreras-Navarrete, J.J., et al., Superficies y Vacio, (2015) 111-114.
- [41] Singh, C., et al., Secondary Singh, C., et al., Ceramics International, (2015) 3595-3604.
- [42] Li, Y., et al., Secondary Li, Y., et al., Applied surface science, (2012) 3659-3666.
- [43] Hazarika, M., P. Chinnamuthu, and J. Borah, Secondary Hazarika, M., P. Chinnamuthu, and J. Borah, Journal of Materials Science: Materials in Electronics, (2018) 12231-12240.
- [44] Yakubu, A., et al., Secondary Yakubu, A., et al., Physical Science International Journal, (2015).
- [45] Anukool, W., et al., Secondary Anukool, W., et al., Applied Physics A, (2022) 1-10.
- [46] Hutamaningtyas, E., A. Wijayanta, and B. Purnama. FTIR and structural properties of co-precipitated cobalt ferrite nano particles. in Journal of Physics: Conference Series. 2016. IOP Publishing.
- [47] Hezam, F., et al., Secondary Hezam, F., et al., Physica B: Condensed Matter, (2020) 412389.
- [48] Wabaidur, S.M., et al., Secondary Wabaidur, S.M., et al., Journal of Molecular Liquids, (2020) 113916.

- [49] Routray, K.L., S. Saha, and D. Behera, Secondary Routray, K.L., S. Saha, and D. Behera, *Materials Science and Engineering: B*, (2017) 199-205.
- [50] Contreras-Navarrete, J., et al., Secondary Contreras-Navarrete, J., et al., *Superficies y vacío*, (2015) 111-114.
- [51] Parashar, J., et al., Secondary Parashar, J., et al., *Journal of Magnetism and Magnetic Materials*, (2015) 105-110.
- [52] Kambale, R., et al., Secondary Kambale, R., et al., *Smart materials and structures*, (2009) 085014.
- [53] Ahmed, I., et al., Secondary Ahmed, I., et al., *Materials Research Bulletin*, (2022) 111687.
- [54] Chahar, M., V. Sharma, and O. Thakur, Secondary Chahar, M., V. Sharma, and O. Thakur, *Journal of Nanoparticle Research*, (2022) 1-13.
- [55] Yasmin, N., et al., Secondary Yasmin, N., et al., *Journal of Alloys and Compounds*, (2019) 962-968.
- [56] Akhtar, M.N., et al., Secondary Akhtar, M.N., et al., *Ceramics International*, (2014) 15821-15829.
- [57] Guerra, V., C. Wan, and T. McNally, Secondary Guerra, V., C. Wan, and T. McNally, *Progress in Materials Science*, (2019) 170-186.
- [58] Yu, K., et al., Secondary Yu, K., et al., *Advanced Engineering Materials*, (2018) 1700543.